Time-Varying Manual Control Identification in a Stall Recovery Task under Different Simulator Motion Conditions

Alexandru Popovici*
San Jose State University, NASA Ames Research Center

Peter M. T. Zaal†
San Jose State University, NASA Ames Research Center

Marc A. Pieters‡
San Jose State University, NASA Ames Research Center, and Delft University of Technology

This paper adds data to help the development of simulator motion cueing guidelines for stall recovery training by identifying time-varying manual control behavior in a stall recovery task under different simulator motion conditions. A study was conducted with seventeen general aviation pilots in the NASA Ames Vertical Motion Simulator. Pilots had to follow a flight director through four stages of a high-altitude stall task. A time-varying identification method was used to quantify how pilot manual control parameters change throughout different stages of the task in both roll and pitch. Four motion configurations were used: no motion, generic hexapod motion, enhanced hexapod motion and full motion. Pilot performance was highest for the enhanced hexapod and full motion configurations in both roll and pitch, and the lowest without motion. In the roll axis, the pilot position gain did not significantly change throughout the stall task, but was the lowest for the condition with no motion. The pilot roll velocity gain was significantly different between motion conditions, the largest difference being found close to the stall point. The enhanced hexapod motion condition had the highest pilot roll velocity gain. In the pitch axis, the pilot position gain was significantly different between time segments but not between motion conditions. The pilot pitch velocity gain was highest for the full motion condition and increased close to the stall point, but did not change significantly for the other motion conditions. Overall, pilot control behavior under enhanced hexapod motion was most similar to that under full aircraft motion. This indicates that motion cueing for stall recovery training on hexapod simulators might be improved by using the principles behind the enhanced hexapod motion configuration.

Nomenclature

A	sinusoid amplitude, deg	K_{trs}	c.g. translational acceleration gain, –
e	error signal, deg	K_v	pilot velocity gain, –
f	forcing function, deg	k	sinusoid index
H_c	controlled dynamics response	MR	motion rating, %
H_f	motion filter response	N	number of sine waves
H_{ol}	open-loop response	n	pilot remnant
H_p	human controller response	n	sinusoid frequency integer factor
h	altitude, ft	r	reference attitude, deg
IAS	indicated airspeed, kts	S_{1-4}	stall task segment
K_d	aircraft dynamics gain, –	s	Laplace operator
K_f	motion filter gain, –	T	thrust, lbf
K_p	pilot position gain, –	T_L	pilot lead time constant, s
K_{rtl}	c.g. to p.s. translational acceleration gain, –	t	time, s

*Research Associate, Human Systems Integration Division, NASA Ames Research Center, Moffett Field, CA, 94035; alexandru.popovici@nasa.gov. Member.

†Senior Research Engineer, Human Systems Integration Division, NASA Ames Research Center, Moffett Field, CA, 94035; peter.m.t.zaal@nasa.gov. Member.

‡Research Scholar, Human Systems Integration Division, NASA Ames Research Center, Moffett Field, CA, 94035; marc.a.pieters@nasa.gov.

t_{1-4}	stall segment end time, s
u	pilot control input, $-$
α	angle of attack, deg
δ_a	aileron deflection, deg
δ_e	elevator deflection, deg
ζ_f	motion filter damping ratio, $-$
ζ_n	pilot neuromuscular damping ratio, $-$
θ	pitch angle, deg
τ_v	pilot time delay, s
ϕ	roll angle, deg
ϕ	sinusoid phase, rad
φ_m	phase margin, deg
ω_c	crossover frequency, rad s^{-1}
ω_d	aircraft dynamics break frequency, rad s^{-1}
ω_f	motion filter break frequency, rad s^{-1}
ω_n	pilot neuromuscular frequency, rad s^{-1}

Abbreviations

DEKF	dual extended Kalman filter
EH	enhanced hexapod
FM	full motion
GH	generic hexapod
GTM	General Transport Model
MLE	maximum likelihood estimation
NM	no motion
OMCT	Objective Motion Cueing Test
PFD	primary flight display
RMS	root mean square
VAF	variance accounted for
VMS	Vertical Motion Simulator

I. Introduction

This paper identifies time-varying manual control behavior in a stall recovery task under different simulator motion conditions to help develop motion cueing guidelines for stall recovery training. Today, airline pilots only receive training in recognizing and recovering from an approach to stall, but not in full stall recovery. Starting in 2019, airline pilots will be required to perform full stall recovery training in flight simulators.[1] However, most training simulators are not set up to provide this training currently, as they do not accurately represent aircraft behavior in upset situations that take the aircraft out of its normal flight envelope.[2] Post-stall aircraft models need to be implemented to correctly simulate the aircraft response after the stall point. In addition, motion cues need to adequately represent this response to ensure the skills learned in simulator training are directly usable in real flight.

Many previous studies investigated the effects of motion cues on manual control skills in different tasks and environments.[3–8] These studies mostly focused on the identification of time-invariant control behavior in single-axis tasks with constant task variables, a limitation largely imposed by the human control behavior identification techniques available at the time. However, under the highly variable conditions in a stall recovery maneuver, pilot manual control behavior is expected to vary significantly due to changes in control effectiveness and aircraft dynamic behavior. The direct applicability of previous pilot behavioral observations in motion flight simulation studies to this scenario might not be straightforward. In the last decades, some progress has been made to identify control behavior under time-varying conditions or in real flight tasks.[9–12] However, the developed approaches either do not allow for a direct estimation of pilot model parameters from time-domain signals, or require a priori assumptions about the changes in manual control parameters. Recently, a new parameter estimation technique based on a dual extended Kalman filter (DEKF) was developed that allows for the direct estimation of pilot model parameters in time-varying tasks such as a stall recovery.[13]

This paper adds data to the current literature as follows. It is the first study to utilize a novel pilot modeling and identification technique based on a DEKF that allows for the direct estimation of pilot control behavior parameters in time-varying tasks such as a stall recovery. Second, using this technique, pilots' adaptation to different simulator motion settings in different segments of a stall recovery maneuver was investigated. Third, this study used the NASA Vertical Motion Simulator (VMS), which allows for inclusion of a full motion condition that represents real aircraft motion. Last, a sufficiently large pilot pool added statistical reliability to the results.

The paper is structured as follows. The stall recovery task is described in Section II, after which the experiment setup is discussed in Section III. The results are provided in Section IV, followed by a discussion and conclusions in Sections V and VI, respectively.

II. Control Task

Pilots performed a high-altitude stall recovery task while compensating for disturbances in both the roll and pitch degrees of freedom simultaneously. A flight director on a primary flight display (PFD) guided the pilots through the stall maneuver. A block diagram of the control task is depicted in Fig. 1.

Aircraft roll and pitch attitudes ϕ and θ were subtracted from the desired roll and pitch attitudes r_ϕ and r_θ to

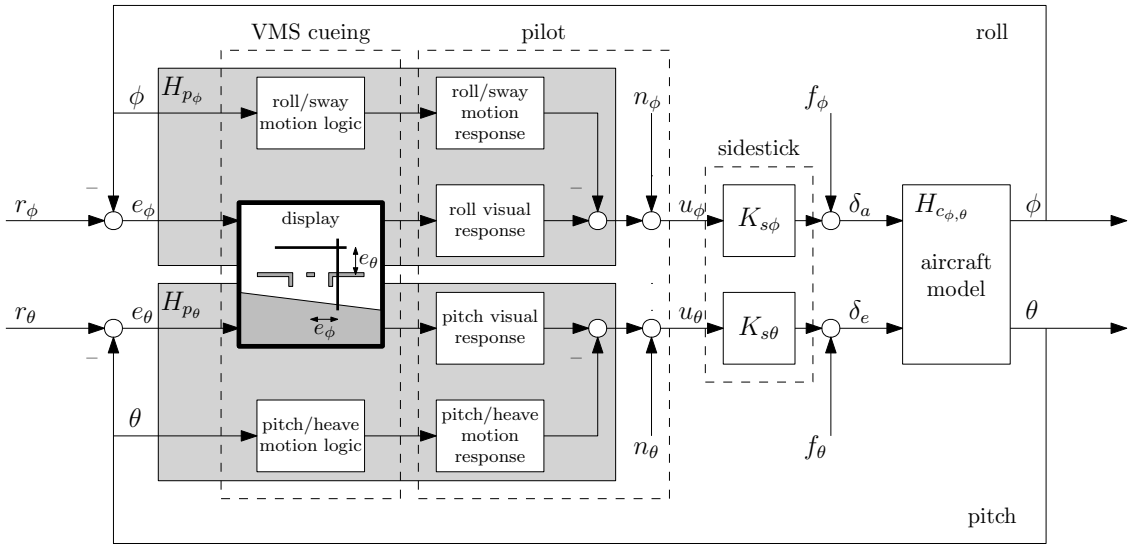

Figure 1. Closed-loop control task.

create roll and pitch errors e_ϕ and e_θ which were indicated by the flight director bars on the PFD. It was pilots' task to minimize the aircraft roll and pitch errors by making control inputs u_ϕ and u_θ using a sidestick with gains $K_{s\phi}$ and $K_{s\theta}$. To allow for the identification of pilot control behavior, two independent disturbance forcing functions $f_{d\phi}$ and $f_{d\theta}$ were used in the roll and pitch axes, respectively, that were a summation of ten sine waves (Section D). The forcing functions induced disturbances similar to atmospheric turbulence. Pilots performed the stall task in the clouds; that is, the out-the-window view did not have any visual features that could be used to determine the attitude of the aircraft.

The stall task was divided into four segments as shown in Fig. 2. In the first segment from 0 to 82 s ($S1$), task parameters remained at the initial trim condition. This segment was used to compare pilot control behavior identified using the newly developed DEKF parameter estimation technique to that identified using traditional methods for time-invariant control behavior. During the second segment from 82 to 124 s ($S2$), pilots flew the aircraft into a stall by following an increased reference pitch attitude. Thrust was set to idle automatically during this segment to get to the stall point faster. The reference pitch attitude dropped below zero in the third segment from 124 to 152 s ($S3$). By following this nose-down reference pitch attitude, the angle of attack was reduced to recover from the stall. During this segment, maximum thrust was applied automatically to regain airspeed faster. After a slow increase of the reference pitch such that secondary stalls did not occur, pilots controlled the aircraft for another 30 seconds around the original pitch trim attitude in the fourth segment ($S4$). The desired roll attitude remained zero during all four segments of the stall recovery task; that is, pilots had to keep the wings level at all times. Segments $S2$ to $S4$ had a transition phase at the beginning in which the reference pitch attitude changed gradually to the new reference value. Data from these transitions were not used in the analysis.

Example recordings for attitude, angle of attack, altitude, airspeed, and thrust during the task are depicted in Fig. 3. The reference signals for roll and pitch are also provided in the top two plots. The transition phases are the areas in between the dashed vertical lines in each plot. Fig. 3 shows that the altitude and airspeed remained approximately constant during $S1$. In $S2$, altitude increased, indicated airspeed decreased, and angle of attack increased gradually up to the critical angle of attack around 16 deg. During the recovery in $S3$, the angle of attack rapidly decreased, altitude decreased and airspeed increased. Finally, in the last segment, the reference pitch attitude had the same value as in the first segment. Angle of attack remained approximately constant, altitude increased, and airspeed decreased slightly.

A. Aircraft Model

The General Transport Model (GTM) was used to simulate the aircraft dynamics. This full-scale simulation model is representative of a generic aircraft similar to a Boeing 757, and includes accurate post-stall dynamics.[14–16] This model was developed from a sub-scale polynomial aerodynamic database, extended to cover the stall regime with wind-tunnel and spin-tunnel test data. The model was further adapted to represent a full-scale aircraft by making Reynolds Number corrections. The model used a basic yaw damper. All other stability and control augmentation functions were

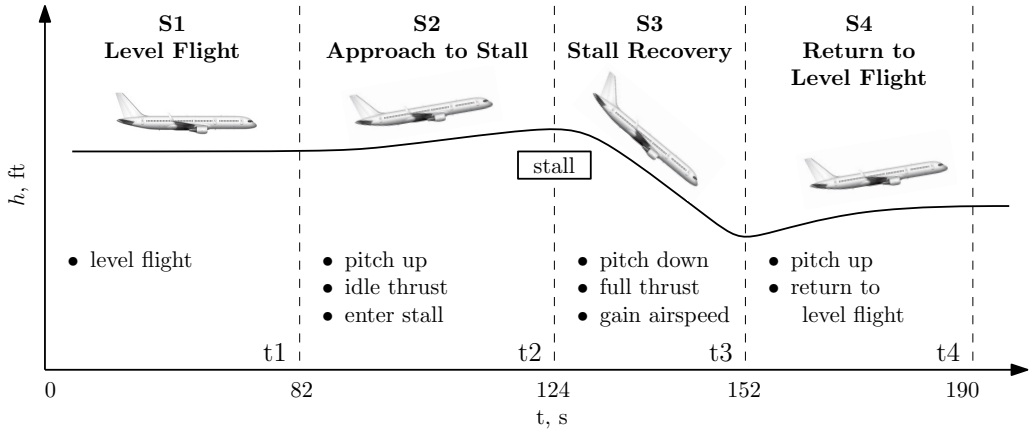

Figure 2. Stall task segments.

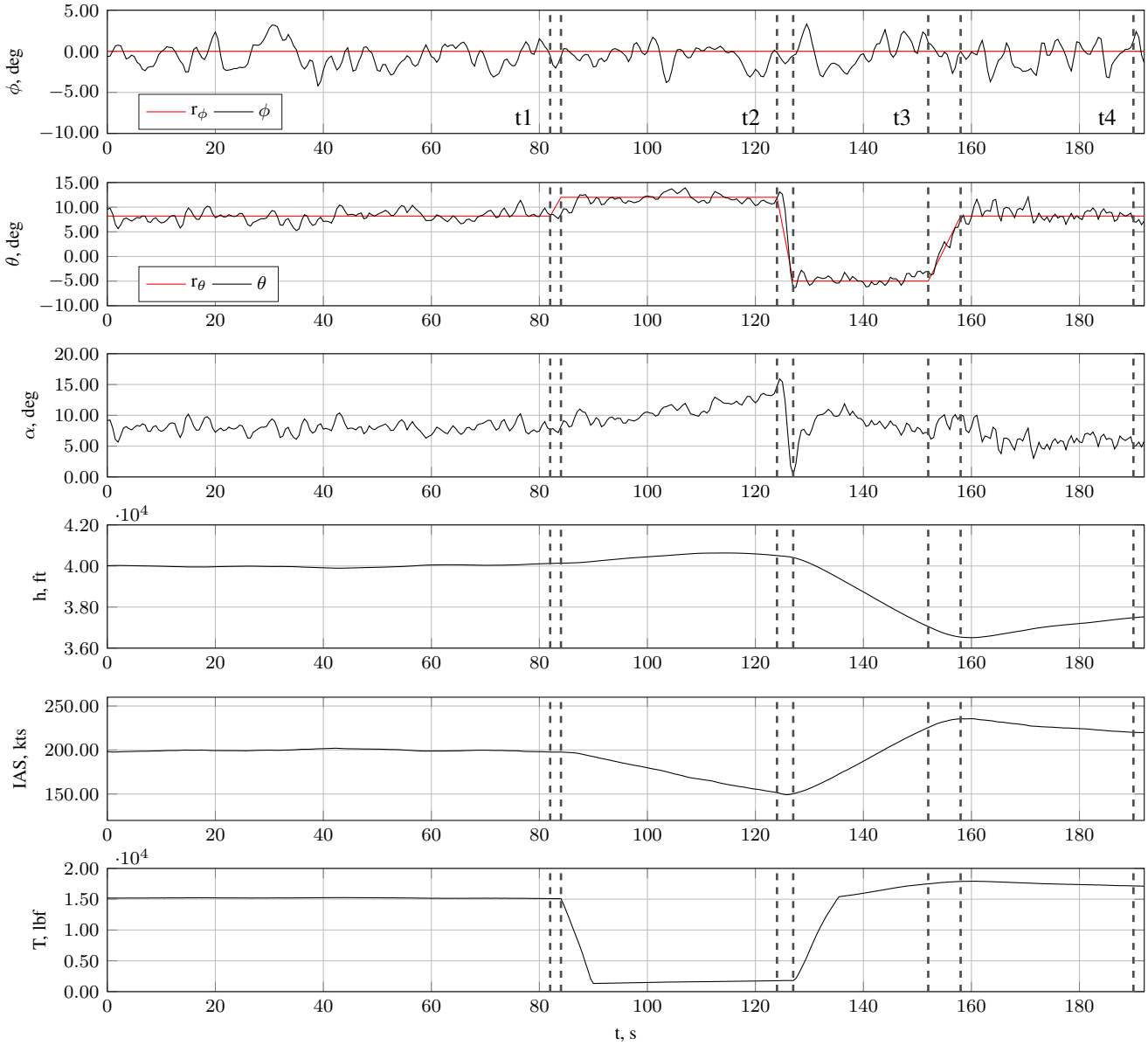

Figure 3. Flight variable recordings.

switched off. The simulation model was implemented in the FLTz simulation environment.[17] At the start of each run the aircraft was trimmed at an altitude of 40,000 ft and a true airspeed of 382 kts. The gross weight of the airplane was 185,000 lbs.

B. Pilot Model

From a control-theoretic perspective, the visual and motion cues in roll and pitch were the inputs to the pilot model and the control inputs were the outputs (Fig. 1). This warrants the identification of a pilot visual and motion response channel in both degrees of freedom. However, the DEKF parameter estimation technique developed in Ref. 13 currently only allows for the identification of a single channel. This means only a lumped response function, combining the visual and motion responses, could be identified. For different reasons, this approach was also taken in previous research investigating the effects of motion cues on pilot control behavior.[18] Cross coupling in pilot control behavior between roll and pitch was not modeled explicitly.

Using the recorded error and control input signals in roll and pitch, the parameters of a pilot model with response functions H_{p_ϕ} and H_{p_θ} were identified using the DEKF parameter estimation technique. The differences between the pilot model response function outputs and the measured pilot control inputs were the remnants (n_ϕ and n_θ), which account for nonlinear behavior and noise. Note that visual display and simulator motion dynamics are also captured by the pilot response functions.

A human operator adapts his or her control behavior to the controlled dynamics such that the combined human operator controlled dynamics open-loop response approximates a single integrator in the region of the crossover frequency, according to the crossover model theorem.[19] Because of the typical characteristics of the transport aircraft dynamics used, the human operator was required to generate lead, especially closer to the stall point when the dynamics become more unstable. Hence, the pilot transfer functions in both roll and pitch were defined by:

$$H_{p_\phi}(s,t) = H_{p_\theta}(s,t) = (K_p(t) + K_v(t)s)e^{-\tau_v s}\frac{\omega_n^2(t)}{s^2 + 2\zeta_n(t)\omega_n(t)s + \omega_n^2(t)} \tag{1}$$

in which the pilot equalization dynamics are characterized by the pilot position gain K_p and the pilot rate gain K_v, or the more commonly used lead time constant T_L. In Eq. (1), $K_v = K_p T_L$. Note that $1/T_L$ defines the frequency where lead starts to be generated. Human controller limitations are captured by the time delay τ_v, neuromuscular frequency ω_{nm}, and neuromuscular damping ζ_{nm}. In order to estimate these parameters using the DEKF technique, the transfer function in Eq. (1) had to be converted to a state-space representation using a 3rd order Padé approximation for the time delay.[13] Furthermore, the time delay was kept constant to minimize the possibility of filter divergence in case not enough control input was provided.

C. Open-Loop Dynamics

Using the control diagram in Fig. 1, the open-loop responses for both roll and pitch were defined by:

$$H_{ol_{\phi,\theta}}(s,t) = H_{p_{\phi,\theta}}(s,t)K_{s_{\phi,\theta}}H_{c_{\phi,\theta}}(s,t) \tag{2}$$

The crossover frequency ($\omega_{c_{\phi,\theta}}$) is the frequency where the magnitude of the open-loop response is 1.0. At this crossover frequency, the phase difference from -180 degrees is the phase margin ($\varphi_{m_{\phi,\theta}}$).

A frequency response of the aircraft dynamics was necessary to compute the open-loop characteristics of the pilot-aircraft system using Eq. (2). The approach was to use a highly simplified form of the aircraft dynamics:

$$H_d(s,t) = \frac{K_d(t)}{s(s + \omega_d(t))} \tag{3}$$

where K_d is the aircraft dynamics gain and ω_d the break frequency where the aircraft response transitions from a single integrator to a double integrator. Both the gain and break frequency were time variant and estimated using an extended Kalman filter technique.

D. Forcing Functions

The pitch and roll forcing functions were sum-of-sines signals defined by Eq. (4), with $A(k)$, $\omega(k)$ and $\phi(k)$ the amplitude, frequency and phase of the k^{th} sine in f_θ or f_ϕ, respectively. $N = 10$ represents the number of sine waves.

Table 1. Forcing function properties.

	Pitch Disturbance, f_θ				Roll Disturbance, f_ϕ			
k	n_ϕ	ω_ϕ	A_ϕ	ϕ_ϕ	n_θ	ω_θ	A_θ	ϕ_θ
–	–	rad s^{-1}	deg	rad	–	rad s^{-1}	deg	rad
1	3	0.230	0.0030	0.9164	2	0.153	0.0030	1.7664
2	7	0.537	0.0030	2.0647	5	0.384	0.0030	0.8532
3	13	0.997	0.0030	1.2614	11	0.844	0.0030	-2.2495
4	27	2.071	0.0030	1.5388	23	1.764	0.0030	-1.0488
5	41	3.145	0.0036	0.6213	37	2.838	0.0037	1.9860
6	53	4.065	0.0040	0.7320	51	3.912	0.0043	-1.0641
7	73	5.599	0.0046	-2.6738	71	5.446	0.0050	1.8933
8	103	7.900	0.0058	-1.5389	101	7.747	0.0064	1.9704
9	139	10.661	0.0077	-2.7371	137	10.508	0.0085	-0.0342
10	174	13.346	0.0101	-2.1734	171	13.116	0.0110	-2.1796

$$f(t) = \sum_{k=1}^{N} A(k) sin[\omega(k)t + \phi(k)] \tag{4}$$

Two disturbance forcing functions were present, one for roll and one for pitch. A summary of all forcing function parameters can be found in Table 1.

The sinusoid frequencies were all integer multiples of the measurement time base frequency, ω = 0.0767 rad/s. The selected integer multiples were used in earlier experiments. They were chosen to fully cover the range of human control at regular intervals on a logarithmic scale.[20]

The amplitudes of the sinusoids were determined using a second-order low-pass filter. The amplitudes of the first four sine waves were manually changed in order to keep the aircraft elevator and aileron deflections within their maximum deflections and the motion of the simulator within the boundaries of the motion envelope throughout the stall task. The final amplitude distribution of the pitch disturbance signal was scaled to obtain a variance of 0.4 deg^2. For roll the variance was higher, 5.0 deg^2, since it was found that the roll error was more difficult to perceive on the PFD.[20] To determine the phase distributions, a high number of phase sets was randomly generated. Two sets were selected that created signals with a Gaussian-like distribution and an average crest factor. The resulting disturbance-rejection task was challenging, but not overly difficult.

E. Simulator Motion

The experiment used four motion configurations. The standard VMS motion algorithm and hardware were used for all four motion configurations. The equivalent time delays of the VMS motion system for the pitch, roll, yaw, longitudinal, lateral and vertical axes are 47, 68, 48, 50, 69 and 67 ms, respectively. More details about the motion algorithm are provided in Ref. 21. The VMS motion logic consists of second-order high-pass filters to attenuate the rotational and translational aircraft model accelerations:

$$H_f(s) = K_f \frac{s^2}{s^2 + 2\zeta_f \omega_f s + \omega_f^2} \tag{5}$$

where K_f is the motion gain, and ζ_f and ω_f are the motion filter damping ratio and break frequency, respectively.

The four motion configurations not only differed in motion filter parameter settings, but also in the type of translational accelerations simulated. Translational accelerations at the pilot station are a combination of translational accelerations of the aircraft's center of gravity (c.g.) and translational accelerations as a result of the pilot station (p.s.) rotating with respect to the center of gravity (Fig. 4). Gains on each of the translational acceleration components (K_{trs} and K_{rtl}) allowed for a different weighting of each component.

The four motion conditions were similar to the ones in Ref. 20. In the no-motion condition (NM), the simulator was operating with the motion system engaged; however, with all motion parameters set to zero. In the hexapod motion configurations, the motion was attenuated to fit within the motion space of a typical 60-inch, six-legged hexapod simulator. The generic hexapod condition (GH) provided motion cuing based on the current industry standard. The motion response of the VMS for this condition was matched to the average response of a statistical sample of eight

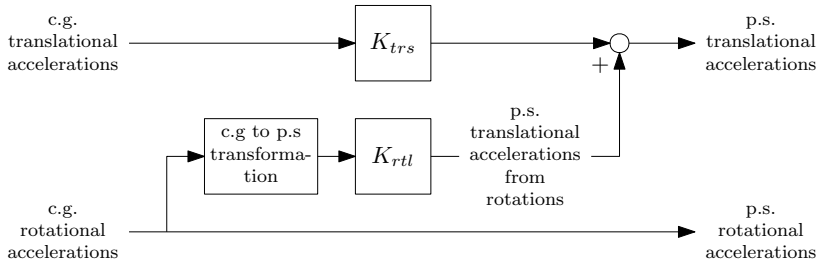

Figure 4. Transformation from center of gravity to pilot station accelerations.

Table 2. Motion logic parameters.

Motion Component Gains			
	GH	EH	FM
K_{trs}	1.00	0.00	1.00
K_{rtl}	1.00	0.75	1.00

Washout Gains			
	GH	EH	FM
K_{fx}	0.58	0.50	0.58
K_{fy}	0.72	1.00	1.00
K_{fz}	0.63	0.80	0.80
K_{fp}	0.74	1.00	1.00
K_{fq}	0.86	0.90	0.90
K_{fr}	0.63	1.00	1.00

Washout Break Frequencies			
	GH	EH	FM
ω_{fx}	2.04	0.80	0.80
ω_{fy}	0.87	0.20	0.20
ω_{fz}	2.76	1.00	1.00
ω_{fp}	1.06	0.20	0.20
ω_{fq}	0.49	0.25	0.25
ω_{fr}	0.77	0.20	0.20

Washout Damping Ratios			
	GH	EH	FM
ζ_{fx}	0.58	0.71	0.71
ζ_{fy}	1.57	0.71	0.71
ζ_{fz}	1.10	0.71	0.71
ζ_{fp}	1.18	0.71	0.71
ζ_{fq}	1.22	0.71	0.71
ζ_{fr}	1.10	0.71	0.71

simulators using the Objective Motion Cueing Test (OMCT).[22] Both the translational acceleration components from the c.g. and as a result of rotations with respect to the c.g. were simulated in this condition.

The enhanced hexapod motion condition (EH) provided motion optimized for stall recovery training based on the findings of our previous experiments. This motion condition only simulated the translational accelerations as a result of rotations with respect to the c.g. Taking out the c.g. component of the total pilot-station translational accelerations resulted in a condition where hardly any attenuation of the remaining accelerations was required, leading to washout gains of 1.00 and break frequencies of 0.20 for most degrees of freedom. The full VMS motion condition (FM) used the entire VMS motion envelope to simulate motion with the highest possible fidelity. In this motion condition both translational acceleration components were simulated with the motion logic parameter settings of condition EH; that is, with minimal attenuation.

Parameter settings for all motion configurations are provided in Table 2. Details on the tilt coordination were omitted from this discussion for brevity; however, tilt coordination was present in each motion configuration. Although an important cue for pilots to recognize an impending stall, buffet motion was not simulated in this experiment, as the main focus was to model the pilot's response to motion cues reflecting the changes in aircraft dynamics during a stall maneuver.

III. Experiment Setup

A. Method

1. Independent Variable

The experiment had a within-subjects design with one independent variable. The independent variable was the motion configuration with four levels: no motion (NM), generic hexapod motion (GH), enhanced hexapod motion (EH), and full VMS motion (FM). The motion configurations are detailed in Section II.E.

2. Apparatus

The experiment was conducted in the VMS with the transport aircraft cab (T-cab), see Fig. 5. This cab has two seats. The left seat had a wheel and column to make control inputs. Participants performed the experiment from the right seat, which had a sidestick on the right side to make control inputs. Rudder pedals were available for both seats, however these were not operational during the experiment. Throttle levers were located in between the seats. The throttles were in auto-throttle mode and were automatically backdriven without pilot inputs. A PFD with representative V-speed

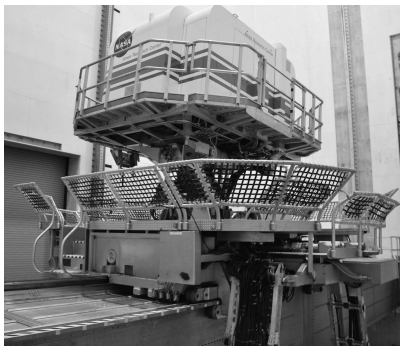

Figure 5. Vertical Motion Simulator.

Figure 6. Cockpit setup.

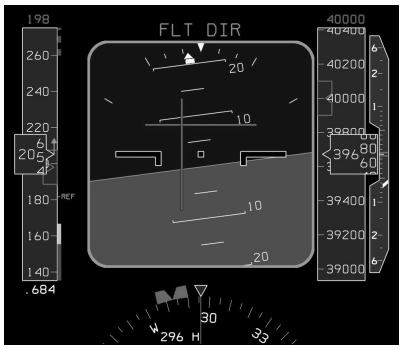

Figure 7. Primary flight display.

markings, a navigation display, and an engine display were located in front of both seats (Fig. 6).

The out-the-window visual cues of T-CAB were collimated and provided by a system that projected a high-quality image on six spherical mirrors. The mirrors formed a dome-like section providing a continuous field-of-view image to both pilots. The out-the-window visual had a 220° horizontal field of view and a 28° vertical field of view (10° up and 18° down). A Rockwell-Collins EPX5000 computer image generator created the out-the-window visual scene. The visual system equivalent time delay was 62 ms.[21] This was in line with the equivalent time delays of the motion system (Section E). The out-the-window visual system provided a visual scene in the clouds, without visual features that could be used to determine the attitude of the aircraft.

3. Procedures

Before the start of the experiment, pilots received an extensive briefing explaining the main purpose of the experiment and the general procedures. Pilots were told the motion settings changed between runs; however, no specifics were given about the different motion conditions. After the briefing, pilots filled out a short questionnaire with questions about their aircraft and simulator experience, after which they signed an informed consent form. After a safety walk-around and an explanation of the relevant simulator cab features, pilots were provided with an example run of the task by the experimenter showing how to compensate for the disturbances more effectively. Pilots were instructed to give smooth and continuous control inputs. To motivate pilots to perform better, they were told the current best performance score (Section 5) and encouraged to improve on it.

Pilots performed eight runs per motion condition (including training runs) for a total of 32 runs. The four motion conditions were presented in random order according to a balanced Latin square design. Each run lasted 190 seconds. The total run time of the experiment was three and a half hours, including briefing and break time. Two or three runs for each condition were performed in between 15-minute breaks. Participants were allowed to take longer brakes if requested. After completing all measurement runs, the final four runs (one run for each motion configuration) were used to gather subjective motion ratings. Pilots were told they could control more freely during these four runs to get a better feel of the motion whilst still performing the stall task. The first run of the last four always used the full motion configuration. Pilots were told this was the baseline full-motion condition. The three remaining motion conditions were then presented randomly and pilots were asked to rate the motion of these conditions against the baseline by providing a percentage between 0 and 100% at the end of each run. They were also asked to provide general comments about the motion.

4. Participants

Seventeen general aviation pilots participated in the experiment. The most experienced pilot had 2,400 flight hours. The average number of flight hours over all participants was 373 hours, with a standard deviation of $\pm$ 582 hours. Furthermore, pilots had an average of 21 hours of flight simulator experience, with a standard deviation of $\pm$ 27 hours. Pilots had flown an average of 48 hours in the past three months, with a standard deviation of $\pm$ 51 hours, both in the simulator and in actual flight. The youngest pilot was 19 years old and the oldest was 38. The average age was 26.9 years, with a standard deviation of $\pm$ 6.1 years. All participants were comfortable with operating the joystick with their right hand. Pilots were compensated for their participation.

5. Dependent Measures

The dependent measures considered in this experiment were motion rating, task performance and control activity, pilot model parameters and pilot-aircraft open-loop characteristics. The motion ratings scored the motion fidelity of the NM, GH, EH conditions against the FM condition, in percentages from 0 (not similar to FM) to 100% (equivalent to FM). The full motion condition had a default rating of 100%.

Pilot performance and control behavior parameters were a function of time. To allow for a comparison of these dependent measures between key points in the stall maneuver, the mean values over the last two seconds of each segment of the stall task ($S1 - S4$) were determined. These time segments are indicated by $t1$ to $t4$ in Fig. 2. Pilot performance and control activity were defined by the root mean square of the attitude errors (RMS_e) and control inputs (RMS_u), respectively, for both roll and pitch, for all four time segments of the stall task.

Pilot model parameters were identified using attitude errors and control inputs in roll and pitch averaged over four runs of each motion condition. A DEKF was used to identify pilot position and velocity gains (K_p, K_v), neuromuscular parameters (ω_n, ζ_n) and a time delay (τ_v).[13] Equalization and neuromuscular parameters were considered time-varying during the run, whereas the time delay was kept constant to minimize the possibility of filter divergence in case not enough control input was provided. Initial parameter estimates were obtained with a maximum likelihood estimation (MLE) method using the first 82 seconds of level flight of the averaged data for each motion condition.[23]

The parameters K_d and ω_d of the aircraft dynamics approximation in Eq. (3) were estimated using an extended Kalman filter. A MLE method was also used in this case to obtain initial parameter estimates from the constant level flight of 82 s in $S1$ to initialize the extended Kalman filter. In this filter, the aircraft parameters were included in the augmented state and estimated for the entire stall recovery maneuver. Finally, the open-loop characteristics were determined using Eq. (2) in order to determine the crossover frequency and phase margin for each motion condition and time segment.

B. Hypotheses

This study used motion configurations similar to those in a previous experiment.[20] The generic hexapod motion condition (GH) had motion similar to what current hexapod training simulators provide. The enhanced hexapod motion condition (EH) eliminated translational c.g. accelerations to allow for increased fidelity of the translational accelerations as a result from rotations about the c.g. and the rotational accelerations themselves; that is, EH had a higher fidelity of the motion cues most important for aircraft control during the stall task compared to GH. For tracking tasks with controlled elements requiring lead equalization, such as the aircraft dynamics used in this study, motion feedback is used by human controllers to reduce the amount of visually generated lead, allowing for better disturbance-rejection performance.[24] The extent to which motion feedback is used is affected by the fidelity of motion stimuli important to the task. Attenuation of these motion cues, either by scaling or high-pass filtering, results in human manual control with lower gains and increased reliance on visual lead, which typically results in worse disturbance-rejection performance. As the stability of the aircraft dynamics decreases closer to the stall point, motion becomes more important to maintain a certain level of performance. A new pilot control behavior identification technique based on a DEKF was used for the first time to investigate how pilot model parameters vary during a stall maneuver under the different motion configurations. Based on these considerations, the literature, and test runs in the VMS, the following hypotheses were formulated:

H1: **Performance of the DEKF** - The DEKF was expected to provide more accurate and consistent results when identifying pilot control behavior in roll compared to pitch as it was easier to perceive and act on roll disturbances. In addition, pitch control inputs had to be adjusted for the DEKF procedure as the measurements were not centered around zero.

H2: **General Effects of Motion on Control Behavior** - Pilot control behavior in the EH motion condition was expected to be more similar to the FM condition compared to GH. Pilot velocity gains were expected to be higher under the motion configurations with higher motion gains and lower break-frequencies (EH and FM), leading to higher open-loop crossover frequencies and lower phase margins. It was anticipated pilots would have the smallest disturbance-rejection error (RMS_e) in the EH and FM conditions and the largest in the NM condition.

H3: **Pilot Adaptations to Changing Dynamics** - It was anticipated that pilots' control behavior and use of motion cues would adapt to the changing aircraft dynamics and conditions throughout the stall task. As the aircraft dynamics become more unstable close to the stall point ($t2$), the pilot velocity gain was expected to increase

while the pilot position gain was not expected to change, resulting in a higher emphasis on visually generated lead.

H4: **Differences Between Motion Configurations over Time** - It was hypothesized that differences in pilot control behavior and performance between the different motion configurations would increase closer to the stall point as motion cues become more important to maintain the same level of disturbance-rejection performance.

IV. Results

This section presents the combined results of 17 pilots that participated in the experiment. Error bar plots depict means and 95% confidence intervals over all pilots for each motion condition and time segment after the data was corrected for between-subject variability. For time-varying dependent variables, means and confidence intervals were calculated from data of the last 2 seconds of each stall segment ($S1$, $S2$, $S3$ and $S4$), see Fig. 2.

A two-way repeated measures analysis of variance (ANOVA) was performed to detect statistically significant interactions between motion configuration and time segment of the stall recovery maneuver (motion $\times$ time) for each dependent measure, or the simple main effects of motion or time. The four levels of motion were: no motion (NM), generic hexapod (GH), enhanced hexapod (EH), and full motion (FM). The four time intervals during the stall recovery maneuver were: level flight ($t1$), approach to stall ($t2$), dive ($t3$), and recovery ($t4$). Pilot time delays for both pitch and roll were considered constant and motion ratings were considered for the entire stall task only. Therefore, a one-way ANOVA was performed for these variables to investigate significant differences between motion conditions only. An overview of the main statistical test results is given in Table 3.

Data from certain pilots were removed due to inaccurate parameter estimates. No outliers were present, as no studentized residuals were outside $\pm$ 3 standard deviations from the mean for each dependent variable.

A. Motion Ratings

In Fig. 8, pilot subjective motion ratings (MR) are presented. A one-way repeated measures ANOVA was performed to investigate the effect of motion condition on subjective motion perception. The FM condition was rated at 100% by default, and the other motion conditions had to be compared relative to this condition. There was a statistically significant effect of motion ($p < 0.001$), see Table 3. Post-hoc analysis with a Bonferroni adjustment showed that MR increased from 0.6% for NM to 66.6% for GH ($p < 0.001$), to 80.4% in EH ($p < 0.001$), and to 100.0% for FM ($p < 0.001$). There was no significant difference in motion ratings between GH and EH ($p = 0.082$). MR significantly increased from 66.6 in GH to 100.0 in FM ($p < 0.001$). Lastly, motion ratings significantly increased from 80.4 in GH to 100.0 in FM.

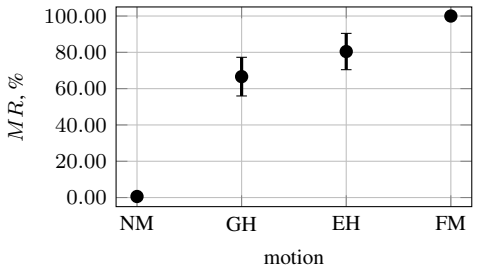

Figure 8. Motion ratings.

B. Pilot Performance and Control Activity

Roll error and control input RMS are presented in Fig. 9. A lower RMS_e and RMS_u indicate better performance and lower control activity, respectively. In Fig. 9a, no statistically significant two-way interaction between motion and time was found for the RMS of the roll error signal. The main effect of motion introduced significant differences in RMS_e between conditions ($p = 0.001$). Post-hoc analysis with a Bonferroni adjustment indicated a significant decrease from 1.337 deg in the NM condition to 1.030 deg in the EH condition ($p = 0.007$), and to 1.035 deg in the FM condition ($p = 0.011$). RMS_e also significantly decreased from 1.168 deg in GH to 1.030 in EH ($p < 0.001$) and to 1.035 in FM ($p < 0.001$). No significant difference was found between the EH and FM conditions ($p = 1.000$). The main effect of time also introduced a significant difference in RMS_e ($p = 0.001$). Post-hoc analysis revealed that the RMS_e increased significantly from 1.057 deg in $t1$ to 1.268 deg in $t4$ ($p < 0.001$), but did not change significantly compared to $t2$ ($p = 0.380$) and $t3$ ($p = 1.000$).

Control input RMS in the roll axis is shown in Fig. 9b. No statistically significant two-way interaction was found between motion and time ($p = 0.119$). The main effect of motion was statistically significant. Post-hoc analysis with a Bonferroni adjustment showed that RMS_u increased from 0.026 in NM to 0.032 in GH, EH and FM ($p < 0.001$).

Table 3. Summary of main statistical test results.

Measure	motion			time			motion × time		
	df	*F*	*p*	*df*	*F*	*p*	*df*	*F*	*p*
MR	3.0,48.0	176.680	<0.001	-	-	-	-	-	-
				Roll					
RMS_e	1.2,19.5^{gg}	12.860	0.001	1.8,28.7^{gg}	9.830	0.001	1.5, 24.6^{gg}	2.243	0.137
RMS_u	3.0,48.0	20.290	<0.001	2.1,34.5^{gg}	16.026	<0.001	3.2, 51.4^{gg}	2.016	0.119
K_p	2.0,26.3^{gg}	2.839	0.076	2.0,26.0^{gg}	14.259	<0.001	4.8, 62.1^{gg}	1.296	0.278
K_v	3.0,39.0	19.800	<0.001	1.3,16.5^{gg}	43.550	<0.001	4.2, 54.3^{gg}	1.359	0.259
τ_v	3.0,39.0	16.543	<0.001	-	-	-	-	-	-
ω_n	1.7,22.5^{gg}	0.658	0.506	2.0,26.5^{gg}	25.879	<0.001	2.3, 30.2^{gg}	2.072	0.137
ζ_n	1.6,20.8^{gg}	6.216	0.011	3.0,39.0	2.013	0.128	9.0,117.0	1.741	0.087
ω_c	1.9,28.4^{gg}	8.736	0.001	3.0,45.0	18.182	< 0.001	9.0,135.0	1.873	0.061
φ_m	1.8,27.4^{gg}	7.466	0.003	1.8,27.0^{gg}	5.866	0.009	1.9, 29.5^{gg}	2.216	0.128
				Pitch					
RMS_e	1.4,22.4^{gg}	18.625	<0.001	3.0,48.0	11.966	<0.001	9.0,144.0	3.285	0.001
RMS_u	1.5,24.8^{gg}	28.345	<0.001	3.0,48.0	37.400	<0.001	4.5, 72.6^{gg}	7.221	<0.001
K_p	3.0,21.0	1.234	0.322	3.0,21.0	84.871	<0.001	3.4, 23.9^{gg}	2.615	0.068
K_v	3.0,48.0	24.727	< 0.001	3.0,48.0	15.849	< 0.001	9.0,144.0	2.253	0.022
τ_v	3.0,48.0	69.213	< 0.001	-	-	-	-	-	-
ω_n	1.5,23.5^{gg}	8.740	0.003	1.4,22.2^{gg}	27.352	<0.001	3.9, 30.2^{gg}	3.389	0.015
ζ_n	2.0,33.1^{gg}	7.439	0.002	1.9,30.9^{gg}	2.473	0.103	2.1, 34.1^{gg}	2.198	0.124
ω_c	3.0,30.0	11.389	< 0.001	3.0,30.0	56.979	< 0.001	9.0,90.0	2.956	0.004
φ_m	3.0,27.0	4.174	0.015	3.0,27.0	36.403	<0.001	9.0,81.0	3.376	0.001

gg = Greenhouse-Geisser correction
■ = significant ($p < 0.05$)
□ = not significant ($p \geq 0.05$)

No significant changes were found between the other levels ($p = 1.000$). The main effect of time was also statistically significant for the roll control input RMS ($p < 0.001$). RMS_u increased significantly from 0.029 in $t1$ and $t2$ to 0.032 in $t3$ and $t4$ ($p = 0.003$).

Pitch error and control input RMS are shown in Fig. 10. Fig. 10a depicts the RMS of the error in the pitch axis. A statistically significant two-way interaction was found between motion and time ($p = 0.001$). Simple main effects of motion revealed that, at time $t1$, RMS_e significantly decreased from 0.846 in NM to 0.745 in GH ($p = 0.001$), to 0.723 in EH ($p < 0.001$), and to 0.738 in FM ($p = 0.003$). Also at time $t1$, there was no significant change in RMS_e between GH and EH ($p = 0.882$) and FM ($p = 1.000$). Furthermore, no statistically significant difference was found between EH and FM ($p = 1.000$). At time $t2$, pitch error RMS significantly decreased from 1.009 in NM to 0.776 in GH ($p = 0.001$), to 0.794 in EH ($p = 0.017$) and to 0.745 in FM ($p < 0.001$). There was no significant difference between GH and EH ($p = 1.000$) and FM ($p = 1.000$). Also at time segment $t2$, there was no significant difference between EH and FM ($p = 1.000$). At $t3$ no significant change was present between NM and GH ($p = 0.079$). RMS_e decreased significantly from 1.019 in NM to 0.789 in EH ($p = 0.008$), and to 0.801 in FM ($p = 0.019$). No significant changes were present between GH and EH ($p = 0.978$), and FM ($p = 0.775$). Lastly, at $t3$, there was no significant change between EH and FM ($p = 1.000$). In the last time segment $t4$, pitch RMS_e did not significantly change between NM and GH ($p = 1.000$), but significantly decreased from 0.996 in NM to 0.826 in GH ($p = 0.020$) and did not significantly change between NM and FM ($p = 0.560$). Pitch error RMS significantly decreased from 0.928 in GH to 0.826 in EH ($p = 0.005$) and did not significantly change between GH and FM ($p = 1.000$). There was no significant change between EH and FM ($p = 0.081$). Simple main effects

of time revealed that for NM there was a significant increase in pitch error RMS from 0.846 at $t1$ to 1.009 at $t2$ ($p = 0.043$), to 1.019 at $t3$ ($p = 0.014$) and to 0.996 at $t4$ ($p < 0.001$). RMS_e did not significantly change from $t2$ to $t3$ ($p = 1.000$) and to $t4$ ($p = 1.000$). There was also no significant change between time segments $t3$ and $t4$ ($p = 1.000$). For the GH motion condition, RMS_e did not significantly change between $t1$ and $t2$ ($p = 1.000$), significantly increased from 0.745 in $t1$ to 0.843 in $t3$ ($p = 0.047$), and to 0.928 in $t4$ ($p < 0.001$). There was no significant difference between $t2$ and $t3$ ($p = 0.422$); however, pitch error RMS increased from 0.776 in $t2$ to 0.928 in $t4$ ($p = 0.006$). No significant difference was found between $t3$ and $t4$ ($p = 0.205$). For the EH motion condition, RMS_e significantly increased from 0.723 in $t1$ to 0.826 in $t4$ ($p = 0.015$). No other significant differences were found. For the FM condition, pitch error RMS did not significantly change between $t1$ and $t2$ ($p = 1.000$) and $t3$ ($p = 0.376$), but significantly increased from 0.738 in $t1$ to 0.916 in $t4$ ($p < 0.001$). Pitch error RMS also significantly increased from 0.745 in $t2$ to 0.916 in $t4$ ($p = 0.004$), but there was no significant difference between $t2$ and $t3$ ($p = 0.358$). There were also no significant differences between $t3$ and $t4$ ($p = 0.064$).

Pitch control input RMS is depicted in Fig. 10b. There was a significant two-way interaction between motion condition and time segment ($p < 0.001$). Simple main effects of motion showed that, at $t1$, RMS_u did not significantly change between NM and GH ($p = 0.671$), and EH ($p = 1.000$), but significantly increased from 0.017 in NM to 0.21 in FM ($p < 0.001$). Pitch control input RMS did not significantly change at $t1$ between GH and EH ($p = 0.170$), but significantly increased from 0.018 in GH to 0.021 in FM ($p < 0.001$). There was also a significant increase from 0.017 in the EH condition to 0.021 in the FM condition ($p < 0.001$). At $t2$, there were no significant differences between NM and GH ($p = 1.000$) and EH ($p = 1.000$). There was a significant increase in pitch RMS_u from 0.019 in NM to 0.021 in FM ($p = 0.01$). There were no significant differences between GH and EH ($p = 1.000$), but there was a significant increase from 0.018 in GH to 0.021 in FM ($p < 0.001$). Also at $t2$, there was a significant increase from 0.018 in EH to 0.021 in FM ($p = 0.001$). At $t3$, there was no significant difference between NM and GH ($p = 0.001$) and EH ($p = 0.001$). There was a significant increase from 0.022 in NM to 0.025 in FM ($p = 0.029$). There was no significant difference in RMS_u between GH and EH ($p = 1.000$), but there was a significant increase from 0.21 in GH to 0.025 in FM ($p < 0.001$). Pitch control input RMS increased significantly from 0.021 in EH to 0.025 in FM ($p = 0.001$). At the last time segment, $t4$, there was no significant difference between NM and GH ($p = 1.000$), and EH ($p = 0.907$). There was a significant increase from 0.019 in NM to 0.026 in FM ($p = 0.001$). Pitch control input RMS significantly increased at $t4$ from 0.020 in GH to 0.026 in FM ($p < 0.001$). No significant differences were found between GH and EH ($p = 1.000$). Pitch control input RMS increased from 0.021 in EH to 0.026 in FM ($p < 0.001$). Simple main effects of time showed that for the NM condition, RMS_u did not significantly change from $t1$ to $t2$ ($p = 0.078$), but significantly increased from 0.017 in $t1$ to 0.022 in $t3$ ($p < 0.001$) and to 0.019 in $t4$ ($p = 0.024$). RMS_u significantly increased from 0.019 in $t2$ to 0.022 in $t3$ ($p = 0.001$), but did not significantly change compared to $t4$ ($p = 1.000$). There was a significant decrease from 0.022 in $t3$ to 0.019 in $t4$ ($p = 0.007$). In the GH condition, pitch RMS_u did not significantly change between $t1$ and $t2$ ($p = 1.000$), but increased from 0.018 at $t1$ to 0.021 at $t3$ ($p < 0.001$) and to 0.020 at $t4$ ($p = 0.016$). Pitch control input RMS increased from 0.018 in $t2$ to 0.021 in $t3$ ($p < 0.001$) and to 0.020 in $t4$ ($p = 0.037$). There was no significant difference in the GH condition between $t3$ and $t4$ ($p = 0.384$). For the EH condition, no significant difference was found between $t1$ and $t2$ ($p = 1.000$); however, RMS_u significantly increased from 0.017 in $t1$ to 0.021 in $t3$ ($p < 0.001$) and to 0.021 in $t4$ ($p = 0.001$). RMS_u significantly increased from 0.018 at $t2$ to 0.021 at $t3$ ($p < 0.001$) and to 0.021 at $t4$ ($p = 0.029$). There was no significant change in the EH condition between $t3$ and $t4$ ($p = 1.000$). Finally, in the FM condition, RMS_u did not significantly change between $t1$ and $t2$ ($p = 0.369$), but significantly increased from 0.21 in $t1$ to 0.025 in $t3$ ($p < 0.001$) and to 0.026 in $t4$ ($p < 0.001$). Pitch control input RMS significantly increased from 0.021 in $t2$ to 0.025 in $t3$ ($p < 0.001$) and to 0.026 in $t4$ ($p < 0.001$). There was no significant difference between $t3$ and $t4$ ($p = 0.427$).

C. Pilot Model Parameters

Pilot model parameters in the roll axis are shown in Fig. 11. Roll position gain is shown in Fig. 11a. No statistically significant two-way interaction was found between motion condition and time for the roll position gain ($p = 0.278$). The main effect of motion showed no statistically significant difference ($p = 0.076$). The main effect of time showed a statistically significant change in K_p ($p < 0.001$). Post-hoc analysis with a Bonferroni adjustment indicated that roll position gain did not significantly change between 0.014 in $t1$ and 0.016 in $t2$ ($p = 0.741$) or 0.012 $t3$ ($p = 0.204$), but significantly decreased to 0.011 in $t4$ ($p < 0.001$). Position gain also significantly decreased from 0.016 in $t2$ to 0.012 in $t3$ ($p = 0.009$) and to 0.011 in $t4$ ($p = 0.001$). There was no statistically significant difference in roll position gain between times $t3$ and $t4$.

The roll velocity gain is depicted in Fig. 11b. There was no significant two-way interaction between motion

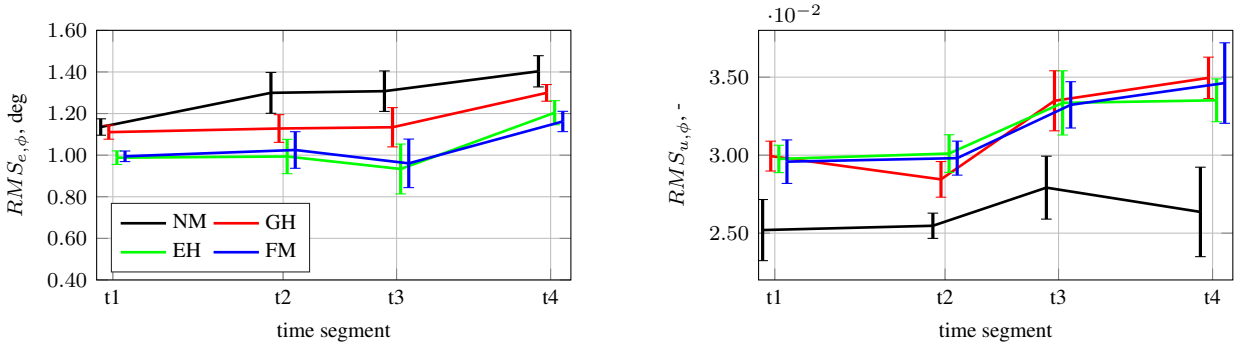

(a) Error RMS.

(b) Control input RMS.

Figure 9. Roll error and control input RMS.

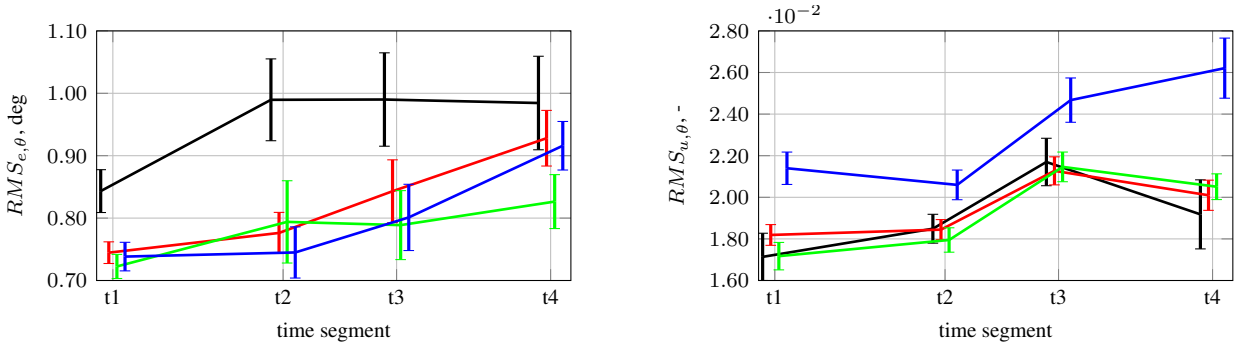

(a) Error RMS.

(b) Control input RMS.

Figure 10. Pitch error and control input RMS.

condition and time for the roll velocity gain. Main effect of motion showed a statistically significant difference ($p < 0.001$). Post-hoc analysis with a Bonferroni adjustment showed that the roll velocity gain increased from 0.009 in NM to 0.011 in GH ($p = 0.001$), to 0.013 in EH ($p < 0.001$), and to 0.012 in FM ($p = 0.001$). K_v significantly increased from 0.011 in GH to 0.013 in EH ($p = 0.021$), but did not significantly change compared to FM. The roll velocity gain did not significantly change between EH and FM. Main effects of time also showed a statistically significant change. Post-hoc analysis revealed that K_v increased from 0.011 in $t1$ to 0.015 in $t2$ ($p = 0.002$), decreased significantly to 0.010 in $t3$ ($p = 0.03$), and to 0.009 in $t4$ ($p < 0.001$). Roll velocity gain decreased from 0.015 in $t2$ to 0.010 in $t3$ ($p < 0.001$) and to 0.009 in $t4$ ($p < 0.001$). It also decreased significantly from 0.010 in $t3$ to 0.009 in $t4$ ($p = 0.001$).

For the neuromuscular frequency ω_n in Fig. 11c, no significant two-way interaction between motion and time was found ($p = 0.137$). The main effect of motion did not show a significant difference in the neuromuscular frequency ($p = 0.506$). However, the main effect of time introduced a significant difference ($p < 0.001$). Post-hoc analysis with Bonferroni adjustment revealed a significant decrease from 5.4 rad/s in $t1$ to 4.86 rad/s in $t2$ ($p < 0.001$) and to 4.97 in $t3$ ($p = 0.002$). No significant difference was found between $t1$ and $t4$ ($p = 0.577$). The neuromuscular frequency did also not change significantly between $t2$ and $t3$ ($p = 1.000$). It increased significantly from 4.86 rad/s in $t2$ to 5.57 rad/s in $t4$ ($p < 0.001$). ω_n increased significantly from 4.97 rad/s in $t3$ to 5.57 rad/s in $t4$ ($p < 0.001$).

The neuromuscular damping ratio is shown in Fig. 11d. No significant two-way interaction between motion condition and time existed ($p = 0.087$). The main effect of time was also not significant ($p = 0.128$). There was a significant main effect of motion ($p = 0.011$). Post-hoc analysis with Bonferroni adjustment showed that the neuromuscular damping ratio decreased significantly from 0.310 in the NM condition to 0.251 in the GH condition ($p = 0.03$), but did not change significantly compared to the EH ($p = 1.000$) and FM ($p = 0.860$) conditions. Neuromuscular damping ratio increased significantly from 0.251 in GH to 0.293 in EH ($p = 0.001$), but did not change significantly compared to FM ($p = 0.159$). There was no significant difference in ζ_n between the EH and

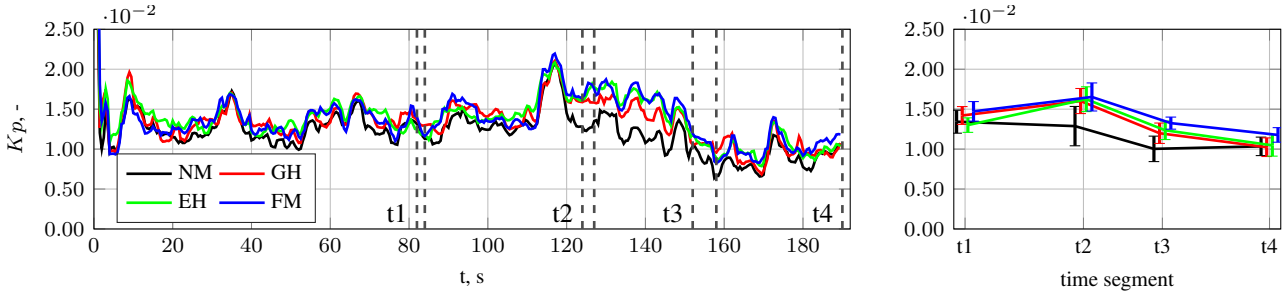

(a) Position gain.

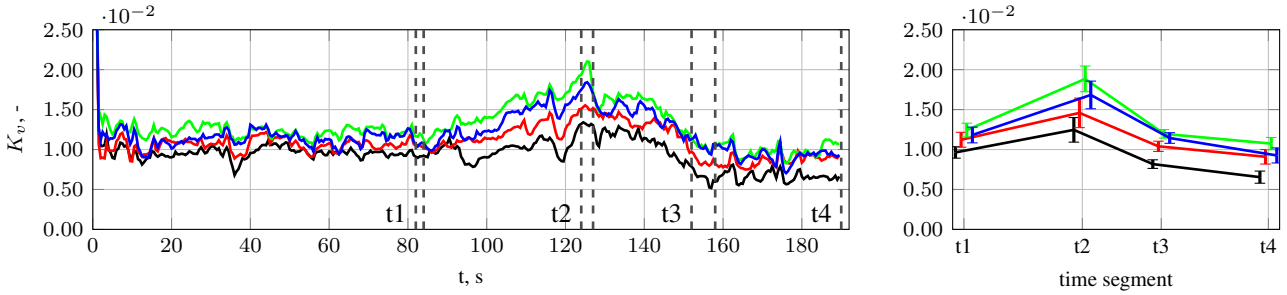

(b) Velocity gain.

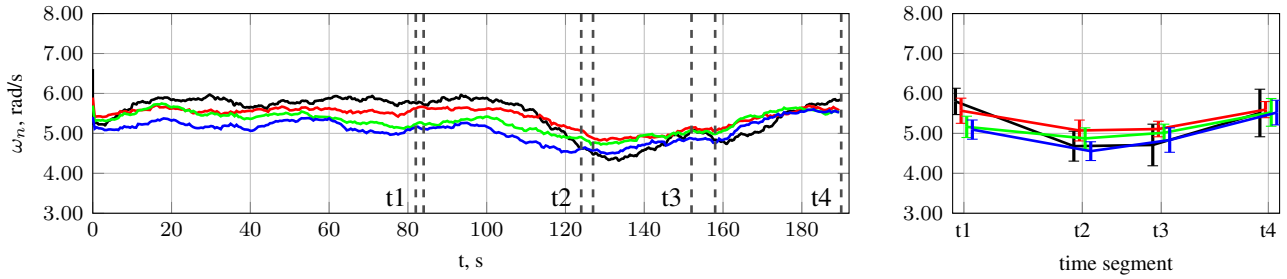

(c) Neuromuscular frequency.

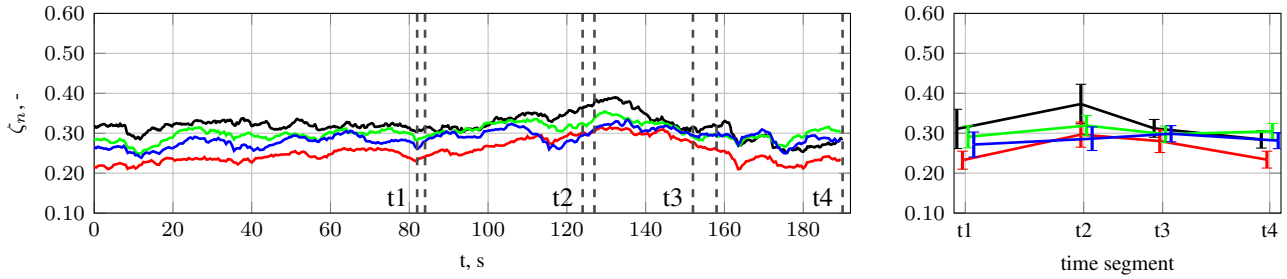

(d) Neuromuscular damping ratio.

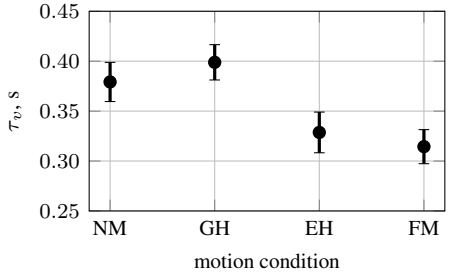

(e) Time delay.

Figure 11. Roll pilot model parameters.

FM motion conditions.

Fig. 11e depicts the pilot roll time delay. The roll time delay significantly changed with motion, as indicated by the one-way ANOVA ($p < 0.001$). For the time delay in the roll axis, post-hoc analysis with Bonferroni adjustment revealed no significant change between the NM and GH conditions ($p = 0.152$). Time delay significantly decreased from 0.374 s in NM to 0.316 s in EH ($p = 0.034$) and to 0.309 s in FM ($p = 0.019$). There was a significant decrease from 0.4 s in GH to 0.316 s in EH ($p = 0.001$) and to 0.309 s in FM ($p < 0.001$). There was no significant change in time delay between EH and FM ($p = 1.000$).

Pitch pilot model parameters are depicted in Fig. 12. There was no significant two-way interaction between motion condition and time for the pitch position gain K_p (0.068). The main effect of motion did also not introduce any significant effects ($p = 0.322$). The main effect of time was statistically significant ($p < 0.001$). Post-hoc analysis with Bonferroni adjustment revealed that pitch position gain did not significantly change between $t1$ and $t2$ ($p = 0.265$), but significantly decreased from 0.012 at $t1$ to 0.002 at $t3$ ($p < 0.001$) and to 0.009 at $t4$ ($p = 0.001$). K_p also significantly decreased from 0.015 at $t2$ to 0.002 at $t3$ ($p < 0.001$) and to 0.006 at $t4$ ($p = 0.007$). Lastly, the pitch position gain significantly increased from 0.002 at $t3$ to 0.009 at $t4$ ($p < 0.001$).

There was a significant two-way interaction between motion condition and time for the pitch velocity gain ($p = 0.022$). The simple main effect of motion indicated that K_v in pitch did not significantly change at $t1$ between NM and GH ($p = 0.216$), and EH ($p = 1.000$). It significantly increased from 0.009 in NM to 0.012 in FM ($p = 0.001$). The pitch velocity gain significantly decreased from 0.11 in GH to 0.009 in EH for $t1$ ($p = 0.003$). There was a significant increase from 0.009 in EH to 0.012 in FM ($p < 0.001$). For $t2$, the pitch velocity gain did not significantly change between NM and GH ($p = 1.000$) and EH ($p = 1.000$); however, it significantly increased from 0.011 in NM to 0.016 in FM ($p = 0.002$). K_v did not significantly change between GH and EH at $t2$ ($p = 0.278$), but it significantly increased from 0.012 in GH to 0.016 in FM ($p = 0.002$). There was also a significant increase from 0.011 in EH to 0.016 in FM ($p < 0.001$). At $t3$, there was no significant change in the pitch velocity gain between NM and GH ($p = 0.165$) and EH ($p = 1.000$), however it significantly increased from 0.009 in NM to 0.013 in FM ($p = 0.001$). There was no significant change between GH and EH ($p = 0.147$) and FM ($p = 0.093$). The pitch velocity gain significantly increased from 0.009 in EH to 0.013 in FM ($p < 0.001$). For the last time segment, $t4$, K_v did not significantly change between NM and GH ($p < 0.065$) and EH ($p = 1.000$), but significantly increased from 0.009 in NM to 0.012 in FM ($p < 0.001$). K_v did not significantly change between GH and EH ($p = 0.847$), but significantly increased from 0.010 in GH to 0.012 in FM ($p = 0.001$). There was also a significant increase at $t4$ from 0.009 in EH to 0.012 in FM ($p < 0.001$). The simple main effect of time revealed that for the NM condition, K_v significantly increased from 0.009 at $t1$ to 0.011 at $t2$, and did not significantly change between $t1$ and $t3$ ($p = 1.000$) and $t4$ ($p = 1.000$). The pitch velocity gain did not significantly change between $t2$ and $t3$ ($p = 0.103$), but significantly decreased from 0.011 in $t2$ to 0.009 in $t4$ ($p = 0.046$). Also for the NM condition, there was no significant difference between $t3$ and $t4$. In the GH condition, no significant difference in pitch velocity gain was found between $t1$ and $t2$ ($p = 0.696$), $t3$ ($p = 1.000$), and $t4$ ($p = 0.569$). There was also no significant difference between $t2$ and $t3$ ($p = 0.165$), but there was a significant decrease from 0.012 in $t2$ to 0.010 in $t4$ ($p = 0.046$). No significant difference was found between $t3$ and $t4$ ($p = 1.000$). In the EH condition, the pitch velocity gain significantly increased from 0.009 in $t1$ to 0.011 in $t2$ ($p = 0.006$), but there was no significant difference between $t1$ and $t3$ ($p = 0.696$) and $t4$ ($p = 1.000$). No other significant differences were found for the EH condition between other time segments. Lastly, for the FM condition, the pitch velocity gain increased from 0.012 at $t1$ to 0.016 at $t2$ ($p = 0.002$), and did not significantly change between $t1$ and $t3$ ($p = 1.000$) and $t4$ ($p = 1.000$). There was a significant decrease from 0.016 at $t2$ to 0.013 at $t3$ ($p = 0.001$) and to 0.012 at $t4$ ($p = 0.002$). No significant difference was found between $t3$ and $t4$ for the FM condition ($p = 1.000$).

A significant two-way interaction was found between motion condition and time for the pitch neuromuscular frequency ($p = 0.015$). The simple main effect of motion showed that at time $t1$, ω_n did not significantly change from the NM to GH condition ($p = 0.873$), but significantly decreased from 8.544 rad/s in NM to 6.549 rad/s in EH ($p < 0.001$). Also at $t1$, there was no significant difference between NM and FM ($p = 0.073$). There were no significant differences between GH and EH ($p = 0.106$) and FM ($p = 0.342$). There was a significant increase in neuromuscular frequency from 6.549 rad/s in EH to 12.701 rad/s in FM (0.009). At time $t2$, there was no significant difference between NM and GH ($p = 0.650$), but ω_n decreased significantly from 7.713 rad/s in NM to 6.375 rad/s in EH ($p = 0.004$). There was also a significant increase in neuromuscular frequency from 7.713 rad/s in NM to 12.362 rad/s in FM ($p = 0.037$). There was no significant difference between the GH and EH conditions ($p = 0.185$) and the FM condition ($p = 0.165$). ω_n significantly increased from 6.374 rad/s in EH to 12.362 rad/s in FM ($p = 0.013$). At time $t3$, the only significant difference found was an increase from 6.312 rad/s in EH to 11.311 rad/s in FM ($p = 0.023$). In the last time segment, $t4$, there was no significant difference between NM and

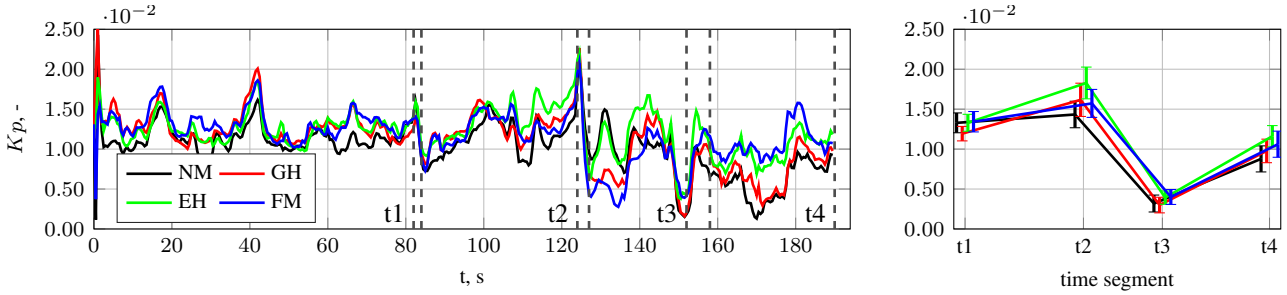

(a) Position gain.

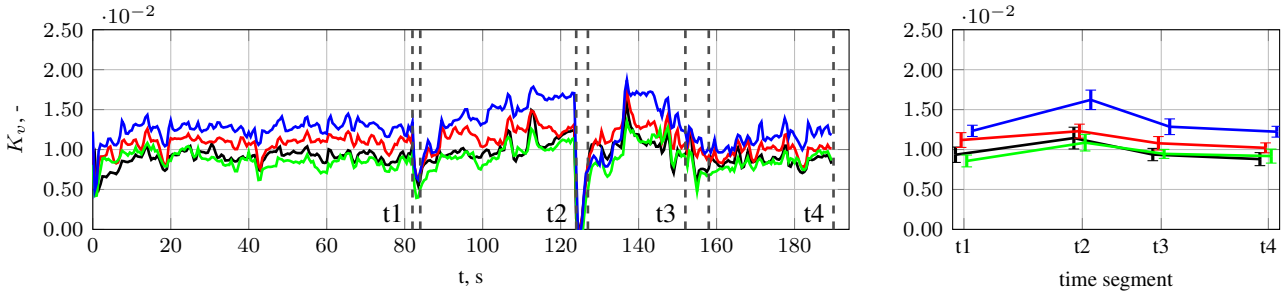

(b) Velocity gain.

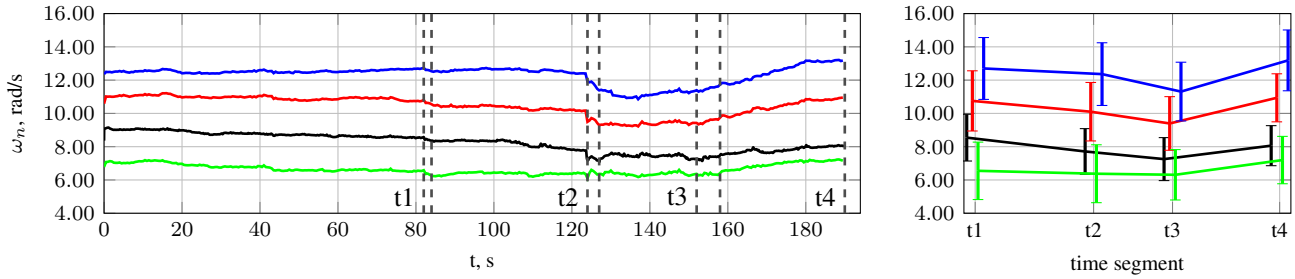

(c) Neuromuscular frequency.

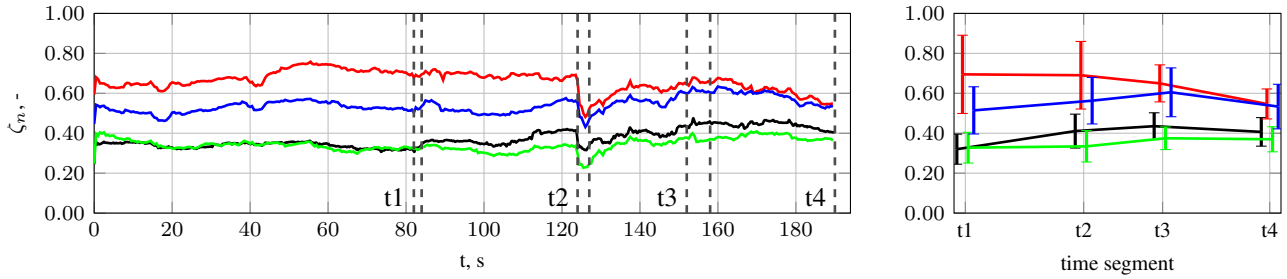

(d) Neuromuscular damping ratio.

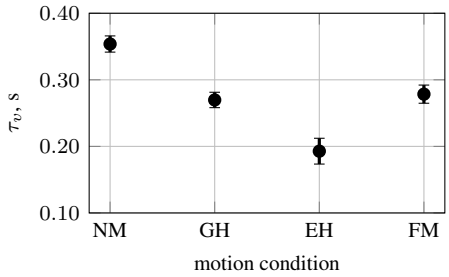

(e) Time delay.

Figure 12. Pitch pilot model parameters.

GH ($p = 0.154$). Pitch neuromuscular frequency significantly decreased from 8.061 rad/s in NM to 7.196 rad/s in EH ($p = 0.035$), and significantly increased to 13.187 rad/s in FM ($p = 0.010$). ω_n significantly decreased from 10.937 rad/s in GH to 7.196 rad/s in EH ($p = 0.048$), but did not significantly change compared to FM ($p = 0.204$). Finally, the pitch neuromuscular frequency significantly increased from 7.196 rad/s in EH to 13.187 rad/s in FM ($p = 0.006$). The simple main effect of time showed that in the NM condition, the pitch neuromuscular frequency significantly decreased from 8.544 rad/s in $t1$ to 7.713 rad/s in $t2$ ($p < 0.001$) and to 7.254 rad/s at $t3$ ($p < 0.001$). There was no significant difference for the NM condition from time $t1$ to time $t4$ ($p = 0.191$). Pitch neuromuscular frequency significantly decreased from 7.713 rad/s in GH to 7.254 rad/s in EH ($p = 0.015$), but there was no significant difference between $t2$ and $t4$ ($p = 0.328$). Also for the NM condition, there was a significant increase from 7.254 rad/s in EH to 8.061 rad/s in FM ($p < 0.001$). For the GH condition, there was a significant decrease from 10.752 rad/s at $t1$ to 10.102 rad/s at $t2$, but there were no significant differences between $t1$ and $t3$ ($p = 0.067$) and $t4$ ($p = 1.000$). The pitch neuromuscular frequency was not significantly different between $t2$ and $t3$ ($p = 0.394$) and $t4$ ($p = 0.307$). There was a significant increase from 9.396 rad/s in $t3$ to 10.937 rad/s in $t4$ ($p < 0.001$). In the EH condition, ω_n did not significantly change between $t1$ and $t2$ ($p = 1.000$) and $t3$ ($p = 1.000$). There was a significant increase in pitch neuromuscular frequency from 6.549 rad/s in $t1$ to 7.196 rad/s in $t4$ ($p = 0.008$). There was no significant difference from $t2$ to $t3$ ($p = 1.000$); however, ω_n significantly increased from 6.375 rad/s in $t2$ to 7.196 rad/s in $t4$ ($p = 0.003$). There was also a significant increase in the EH condition from 6.312 rad/s in $t3$ to 7.196 rad/s in $t4$ ($p < 0.001$). Finally, for the FM motion condition, the pitch neuromuscular frequency did not significantly change from $t1$ to $t2$ ($p = 0.534$), but significantly decreased from 12.701 rad/s in $t1$ to 11.311 rad/s in $t3$ ($p = 0.005$). There was no significant difference between $t1$ and $t4$ ($p = 0.753$). The pitch neuromuscular frequency significantly decreased from 12.362 rad/s at $t2$ to 11.311 rad/s in $t3$ ($p = 0.004$), but did not significantly change compared to $t4$ ($p = 0.063$). Lastly, ω_n significantly increased from 11.311 rad/s in $t3$ to 13.187 rad/s in $t4$ for motion condition FM ($p < 0.001$).

There was no significant two-way interaction between motion condition and time for the neuromuscular damping ratio in the pitch axis ($p = 0.124$). The main effect of motion was statistically significant ($p = 0.002$). Post-hoc analysis with a Bonferroni adjustment revealed that ζ_n significantly increased from 0.393 in NM to 0.645 in GH ($p = 0.029$), but was not significantly different between NM and EH ($p = 0.858$) and FM ($p = 0.213$). There was also a significant decrease from 0.645 in the GH motion condition to 0.352 in the EH motion condition ($p = 0.006$), but no difference between the GH and FM conditions ($p = 1.000$). Finally, there was no significant difference in pitch neuromuscular damping ratio between the EH and FM conditions ($p = 0.053$).

There was a significant difference introduced by motion for the pilot pitch time delay. Post-hoc analysis with Bonferroni adjustment revealed a decrease from 0.354 s in the NM condition to 0.270 s in GH ($p < 0.001$), to 0.193 s in EH ($p < 0.001$) and to 0.278 s in FM ($p < 0.001$). The time delay also significantly decreased from 0.270 s in GH to 0.193 s in EH ($p < 0.001$), but did not significantly change compared to the FM condition ($p = 1.000$). The pitch time delay significantly increased from 0.193 s in the EH condition to 0.278 s in the FM condition ($p < 0.001$).

D. Aircraft Dynamics

Identified roll and pitch aircraft dynamics parameters are shown in Fig. 13 and Fig. 14, respectively. As these aircraft dynamics parameters were estimated with the end goal of determining the time-varying open-loop parameters presented in Section E, no ANOVA was performed. From Figures 13a and 14a, it can be seen that the dynamics gain in both roll and pitch was lower in $t2$ and $t3$; that is, close to the stall point and at the end of the dive. This is in line with the observed reduced control authority around these time segments. The roll dynamics break-frequency first increased from $t1$ to $t2$ after which it decreased in $t3$ and increased again in $t4$ (Fig. 13b). The pitch dynamics break-frequency decreased from $t1$ to $t2$ and then increased slightly in $t3$ and increased further in $t4$ (Fig. 14b). These observation indicate a slight reduction in aircraft roll stability in $t3$, and a reduction in pitch stability mainly in $t2$.

To verify the accuracy of the highly simplified aircraft dynamics representation in Eq. (3), the variance accounted for (VAF) of the modeled aircraft dynamics output for the first 82 seconds of flight in $S1$ using the MLE and EKF methods is depicted in Fig. 15. The VAF is relatively high for both parameter estimation methods, indicating that the simplified dynamics can describe the non-linear aircraft model reasonably well. It can be seen that the VAF is higher using the EKF for both the roll and pitch axes. This is to be expected, since the MLE method assumes constant dynamics, whereas the EKF is able to identify time-varying parameters.

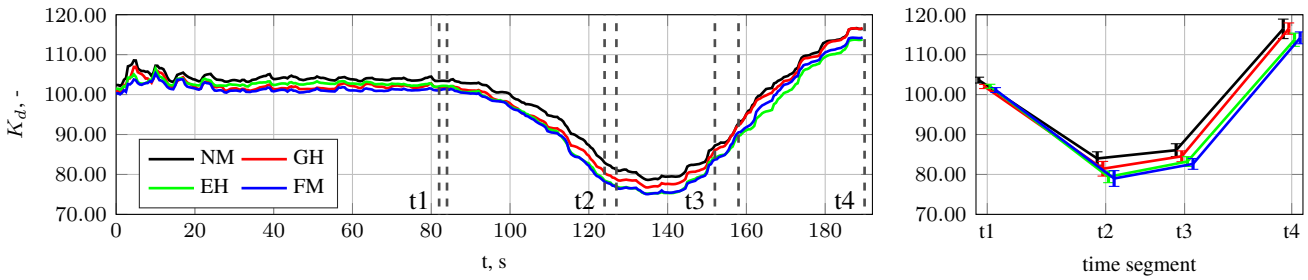

(a) Dynamics gain.

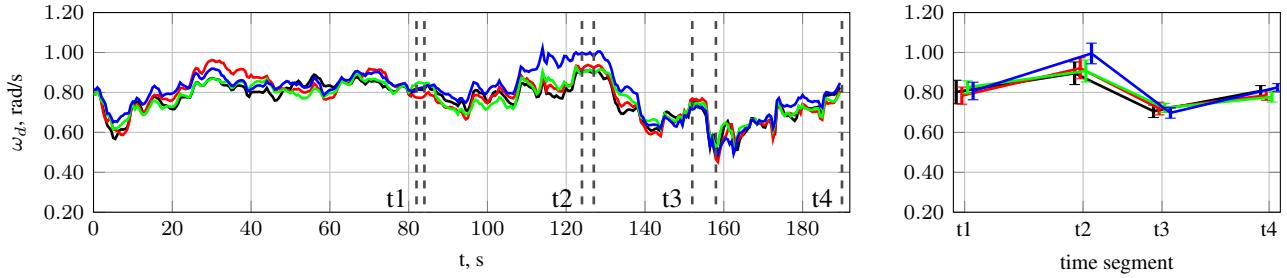

(b) Dynamics break frequency.

Figure 13. Roll dynamics characteristics.

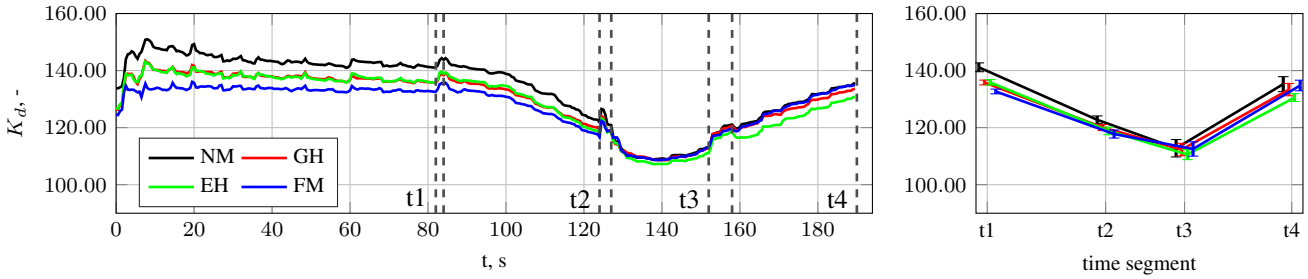

(a) Dynamics gain.

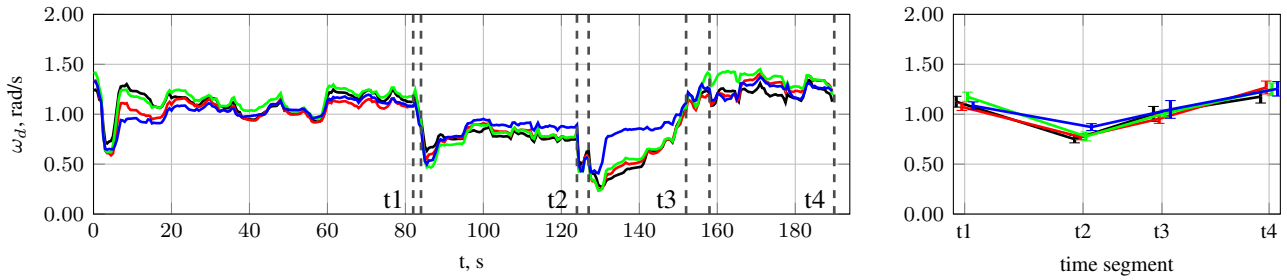

(b) Dynamics break frequency.

Figure 14. Pitch dynamics characteristics.

E. Performance and Stability

Performance and stability in the frequency domain are characterized by the pilot-vehicle transfer function crossover frequency and phase margin in Figures 16 and 17 for roll and pitch, respectively.

There was no significant two-way interaction between motion and time for the roll crossover frequency ($p = 0.061$), see Table 3. The main effect of motion showed a significant result ($p = 0.001$). Post-hoc analysis with a Bonferroni adjustment revealed that ω_c in roll significantly increased from 1.152 rad/s in NM to 1.273 rad/s in GH

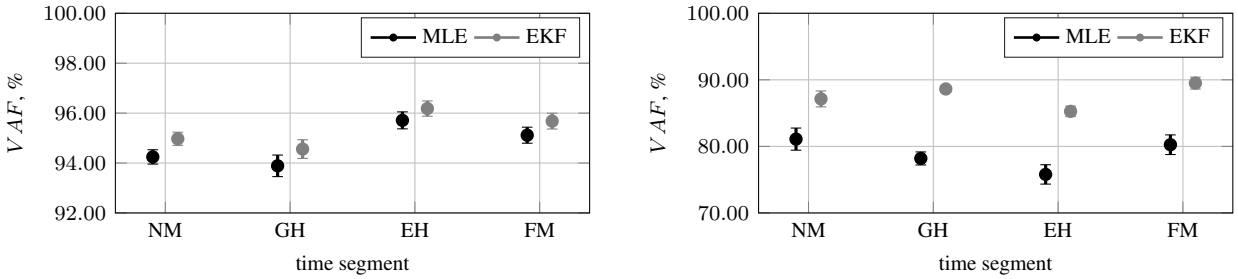

(a) Roll dynamics VAF.

(b) Pitch dynamics VAF.

Figure 15. Variance Accounted For for aircraft identification.

($p = 0.028$) and to 1.368 rad/s in EH ($p = 0.004$), but did not significantly change compared to FM ($p = 0.082$). There was no significant difference in roll crossover frequency between GH and EH ($p = 0.165$) and FM ($p = 1.000$), or between EH and FM ($p = 0.505$). The main effect of time also showed a significant effect ($p < 0.001$). Roll crossover frequency did not significantly change between 1.381 rad/s at $t1$ and 1.359 rad/s at $t2$ ($p = 1.000$), but significantly decreased from 1.381 rad/s at $t1$ to 1.111 rad/s at $t3$ ($p < 0.001$) and to 1.242 rad/s at $t4$ ($p = 0.001$). There was also a significant decrease from 1.359 rad/s at $t2$ to 1.111 rad/s at $t3$ ($p = 0.002$), but no significant difference compared to the roll crossover frequency at $t4$ ($p = 0.153$). Lastly, roll ω_c significantly increased from 1.111 at $t3$ to 1.242 rad/s at $t4$ ($p = 0.005$).

In Fig. 16b, the roll phase margins are shown. There was no significant two-way interaction between motion and time ($p = 0.128$). The main effect of motion showed that there was a significant difference in roll phase margin ($p < 0.003$). Post-hoc analysis with Bonferroni adjustment revealed that roll phase margin significantly increased from 74.720 deg in NM to 79.975 deg in GH ($p = 0.029$), and to 85.481 deg in EH ($p < 0.001$). There was no significant difference between NM and FM ($p = 0.297$). There was also a significant increase from 79.975 deg in GH to 85.481 deg in EH ($p = 0.001$), but no significant difference between GH and FM ($p = 1.000$). Roll phase margin significantly decreased from 85.481 deg in EH to 80.751 deg in FM ($p = 0.028$). The main effect of time also showed a significant difference ($p = 0.009$). Post-hoc analysis with a Bonferroni adjustment showed that roll phase margin significantly increased from 78.821 deg at $t1$ to 87.578 deg at $t2$ ($p = 0.002$), but did not significantly change compared to $t3$ ($p = 1.000$) and $t4$ ($p = 1.000$). The roll phase margin significantly decreased from 87.578 deg in $t2$ to 77.871 deg in $t3$ ($p = 0.011$) and to 76.657 deg in $t4$ ($p = 0.025$). Finally, φ_m in roll did not significantly change between $t3$ and $t4$ ($p = 1.000$).

Fig. 17a shows the crossover frequency for the pitch axis. A significant two-way interaction was found between motion condition and time ($p = 0.004$). The simple main effect of motion revealed that at $t1$, pitch crossover frequency did not significantly change from 1.465 rad/s in NM to 1.519 rad/s in GH ($p = 1.000$), to 1.337 rad/s at EH ($p = 0.845$) and to 1.644 rad/s at FM ($p = 0.087$). The pitch crossover frequency significantly decreased from 1.519 rad/s in GH to 1.337 rad/s in EH ($p = 0.034$) and significantly increased to 1.644 rad/s in FM ($p = 0.046$). There was a significant increase from 1.337 rad/s in EH to 1.644 rad/s in FM. At time $t2$, pitch crossover frequency did not significantly change from 1.616 rad/s in NM to 1.695 rad/s in GH ($p = 1.000$) or to 1.664 rad/s in EH ($p = 1.000$),

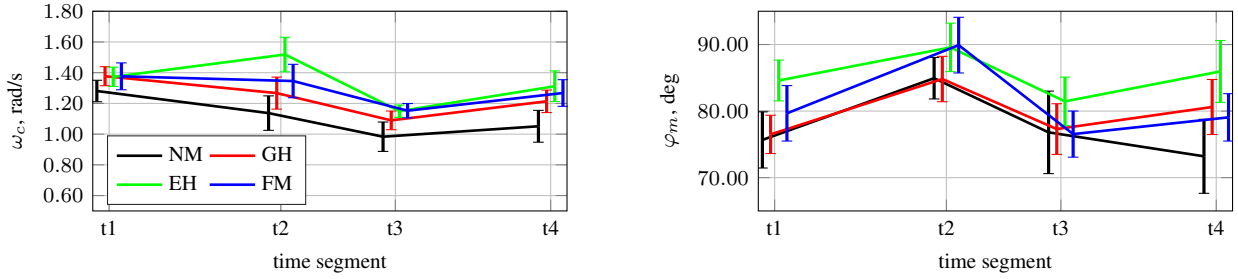

(a) Crossover frequency.

(b) Phase margin.

Figure 16. Roll performance and stability.

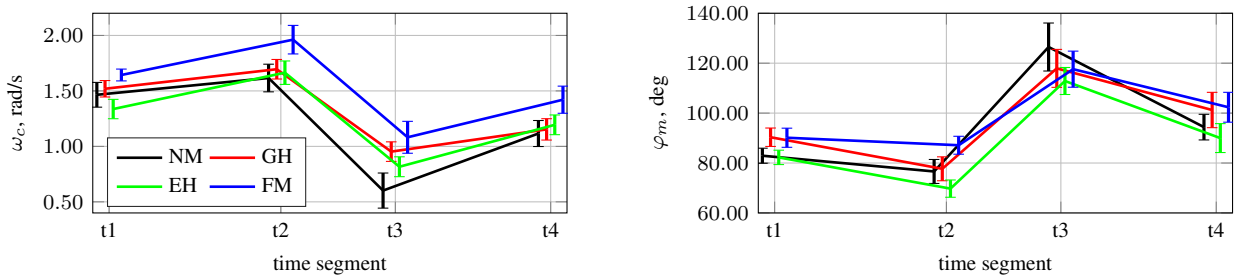

(a) Crossover frequency.

(b) Phase margin.

Figure 17. Pitch performance and stability.

but significantly increased to 1.962 rad/s in FM ($p = 0.014$). There was no significant difference between GH and EH ($p = 1.000$) and FM ($p = 0.063$). There was a significant increase from 1.664 rad/s in EH to 1.962 rad/s in FM ($p = 0.031$). At time segment $t3$, ω_c in pitch significantly increased from 0.691 rad/s for NM to 1.108 rad/s for GH ($p = 0.021$), but did not significantly change compared to EH ($p = 0.206$) and FM ($p = 0.064$). There was no significant difference between GH and EH ($p = 0.269$) and FM ($p = 1.000$). Lastly, no significant change was found between EH and FM ($p = 0.175$). At $t4$, the pitch crossover frequency did not significantly change from 1.116 rad/s in NM to 1.153 rad/s in GH ($p = 1.000$) or to 1.153 rad/s in EH ($p = 1.000$), but significantly increased to 1.421 rads/s for FM ($p = 0.036$). There was no significant difference between GH and EH ($p = 1.000$). A significant increase was found between 1.153 rad/s in GH and 1.421 rad/s in FM ($p = 0.037$). Pitch ω_c was not significantly different between EH and FM ($p = 0.096$). The simple main effect of time revealed that in the NM condition, the pitch crossover frequency was not significantly different between 1.499 rad/s at $t1$ and 1.655 rad/s at $t2$ ($p = 0.297$), but significantly decreased to 0.596 rad/s at $t3$ ($p < 0.001$) and to 1.125 rad/s at $t4$ ($p < 0.001$). There was a significant decrease from 1.655 rad/s at $t2$ to 0.596 rad/s at $t3$ ($p < 0.001$) and to 1.125 rad/s at $t4$ ($p = 0.001$). A significant increase was found from 0.596 rad/s at $t3$ to 1.125 rad/s at $t4$ ($p = 0.001$). In the GH condition, pitch ω_c did not significantly change from 1.530 rad/s at $t1$ to 1.731 rad/s at $t2$ ($p = 0.066$), but significantly decreased to 0.942 rad/s at $t3$ ($p < 0.001$) and to 1.156 rad/s at $t4$ ($p < 0.001$). There was also a significant decrease from 1.731 rad/s at $t2$ to 0.942 rad/s at $t3$ ($p < 0.001$) and to 1.156 rad/s at $t4$ ($p < 0.001$). No significant change was found between $t3$ and $t4$ ($p = 0.334$). In the EH condition, pitch crossover frequency significantly increased from 1.462 rad/s at $t1$ to 1.718 rad/s at $t2$ ($p = 0.023$), significantly decreased to 0.872 rad/s at $t3$ ($p < 0.001$), and did not significantly change compared in $t4$ ($p = 0.244$). There was also a significant decrease from 1.718 rad/s at $t2$ to 0.872 rad/s at $t3$ ($p < 0.001$) and to 1.310 rad/s at $t4$ ($p = 0.001$). Also in the EH condition, pitch ω_c significantly increased from 0.872 rad/s at $t3$ to 1.310 rad/s at $t4$ ($p = 0.002$). Lastly, in the FM condition, the pitch crossover frequency significantly increased from 1.644 rad/s at $t1$ to 1.962 rad/s at $t2$ ($p = 0.003$), significantly decreased to 1.055 rad/s at $t3$ ($p < 0.001$), and significantly decreased to 1.421 rad/s at $t4$ ($p = 0.049$). There was a significant decrease from 1.962 rad/s at $t2$ to 1.055 rad/s at $t3$ ($p < 0.001$) and to 1.421 rad/s at $t4$ ($p < 0.001$). Pitch crossover frequency significantly increased from 1.055 rad/s at $t3$ to 1.421 rad/s at $t4$ ($p = 0.012$).

For the pitch phase margin in Fig. 17b, there was a significant two-way interaction between motion condition and time ($p = 0.001$). The simple main effect of motion showed that at $t1$, there was a significant difference between 82.927 deg in NM and 90.333 deg in GH ($p = 0.039$), but no significant difference between NM and EH ($p = 1.000$) or FM ($p = 0.067$). There was a significant decrease from 90.333 deg in GH to 82.259 deg in EH ($p = 0.020$), but no difference between GH and FM ($p = 1.000$). Also at $t1$, there was a significant increase from 82.259 deg in EH to 90.131 deg in FM ($p = 0.028$). At time $t2$, no significant difference was found for the pitch phase margin between 76.618 deg in NM and 77.688 deg in GH ($p = 1.000$) and 69.745 deg in EH ($p = 0.185$). There was a significant increase from 76.618 deg in NM to 87.124 deg in FM ($p = 0.046$). No significant difference existed between GH and EH ($p = 0.190$); however, the pitch phase margin increased from 77.688 deg in GH to 87.124 deg in FM ($p = 0.034$). Lastly at $t2$, there was a significant increase from 69.745 deg in EH to 87.124 deg in FM ($p < 0.001$). At $t3$, no significant differences between motion conditions were found. The mean phase margin was 126.335 deg for NM, 111.755 for GH, 106.012 deg for EH and 105.594 deg for FM. At time segment $t4$, there were also no significant differences between motion conditions. The mean phase margin was 94.386 deg for NM, 101.241 deg for GH, 89.990 deg for EH and 102.345 deg for FM. The simple main effect of time revealed that, in the NM condition, the pitch phase margin did not significantly change from 83.407 deg at $t1$ to 78.415 deg at $t2$

($p = 1.000$), but increased significantly from 83.407 deg at $t1$ to 127.349 deg at $t3$ ($p < 0.001$) and to 95.286 deg at $t4$ ($p = 0.018$). It also significantly increased from 78.415 deg at $t2$ to 127.349 deg at $t3$ ($p < 0.001$), and to 95.286 deg at $t4$ ($p = 0.003$). Lastly, the pitch phase margin significantly decreased from 127.349 deg at $t3$ to 95.286 deg at $t4$ ($p < 0.001$). For motion condition GH, the phase margin significantly decreased from 89.662 deg at $t1$ to 78.707 deg at $t2$ ($p = 0.008$) and increased to 119.409 deg at $t3$ ($p = 0.002$). It did not significantly change compared to the phase margin at $t4$ ($p = 0.618$). The pitch phase margin significantly increased from 78.707 deg at $t2$ to 119.409 deg at $t3$ ($p =< 0.001$) and to 98.167 deg at $t4$ ($p = 0.016$). Lastly for the GH condition, the pitch phase margin significantly decreased from 119.409 deg at $t3$ to 98.167 deg at $t4$ ($p = 0.007$). In the EH motion condition, the pitch phase margin did not significantly change between 79.621 deg at $t1$ and 70.732 deg at $t2$ ($p = 0.116$) and 85.841 deg at $t4$ ($p = 0.519$). It did increase from 79.621 deg at $t1$ to 107.979 deg at $t3$ ($p = 0.002$). There was also a significant increase from 70.732 deg at $t2$ to 107.979 deg at $t3$ ($p < 0.001$) and to 85.841 deg at $t4$ ($p = 0.041$). The pitch phase margin significantly decreased from 107.979 deg at $t3$ to 85.841 deg at $t4$ ($p = 0.027$). Finally, in the FM condition, the phase margin did not significantly change between 90.402 deg at $t1$ and 88.245 deg at $t2$ ($p = 1.000$), significantly increased to 119.295 deg at $t3$ ($p = 0.001$) and significantly increased to 101.264 deg at $t4$ ($p = 0.010$). It also significantly increased from 88.245 deg at $t2$ to 119.295 deg at $t3$ ($p = 0.001$) and to 101.264 deg at $t4$ ($p = 0.044$). Lastly for the FM condition, pitch phase margin significantly decreased from 119.295 deg at $t3$ to 101.264 deg at $t4$ ($p = 0.047$).

V. Discussion

A stall recovery task was performed under different simulator motion conditions. Pilots had to follow a flight director that guided them through the approach to stall and stall recovery maneuvers. Disturbance forcing functions were added in order to identify pilot control behavior in both pitch and roll axes. The stall task was divided into four segments (Fig. 2). The first segment ($S1$) consisted of a level flight at 40 000 ft. Then, pilots had to pitch up in order to enter a stall ($S2$), after which they entered a dive in order to increase their airspeed and recover from the stall ($S3$). In the last segment ($S4$), pilots had to pull up slowly to recover the airplane to the original level flight condition. Pilots flew the task under four motion conditions: no motion (NM), generic hexapod motion (GH), enhanced hexapod motion (EH), and full motion (FM).

Subjective motion ratings were collected in order to analyze how the motion in the no motion and hexapod motion conditions compared to that in the full motion condition. As expected, the condition with no motion was rated the lowest, followed by the generic hexapod condition and the enhanced hexapod condition. In general, the EH and FM motion conditions felt most similar. However, there was no statistically significant difference between how pilots rated the GH and EH conditions. In the last segment, $S4$, the motion felt more violent than in $S1$, especially for the EH and FM motion configurations. This might be due to the fact that the airspeed and air density were higher in $S4$ compared to $S1$.

Task performance was defined by the RMS of the error signal in both axes. Roll error RMS was the highest for the NM condition, indicating worse performance, and the lowest for the EH and FM conditions, indicating better performance. Furthermore, the roll error RMS slightly increased from $t1$ to $t4$, most likely due to the more violent motion in $t4$ compared to $t1$. Similar trends were observed for the pitch axis. However, for the first three time segments, there was no significant difference in pitch performance between the GH, EH and FM conditions. In the last time segment the best performance was found for the EH motion condition. Control activity was calculated from the RMS of the control input. It is interesting to note that for roll, the lowest control input was in the NM condition, whereas there were no significant differences between the conditions with motion. In the pitch axis however, the highest control input was observed for the FM condition, but no difference was observed for the other three conditions. This could mean that for roll, pilots controlled with more confidence whenever motion was available, whereas in pitch they controlled with more confidence in the full motion case only. This difference between roll and pitch cannot readily be explained.

Pilot model parameters were identified using a DEKF. For the roll position gain, no differences were found between motion conditions during the level flight segments $S1$ and $S4$, however in the approach to stall and dive maneuvers, the roll K_p was the smallest for the NM condition compared to the conditions in which motion was present. No significant differences were found between the flight segments. Roll velocity gain was significantly affected by motion conditions. It was the highest under EH and lowest under NM, indicating that pilots increased their velocity gain with more motion. The reason why the roll velocity gain is highest for the EH and not for the FM condition might be due to increased false tilt motion cues in EH compared to FM. The roll velocity gain increased at the end of $S2$ compared to $S1$, meaning that pilots acted more on velocity information close to stall, probably due to the decreased

aircraft stability close to the stall point. The roll K_v was smaller at the end of the $S4$ segment compared to $S1$, most likely as the aircraft still had not returned fully to the initial trim condition at the beginning of the flight. The neuromuscular frequency ω_n in roll did not change between motion conditions; however, it decreased going from $t1$ to $t2$ and $t3$, and recovered back to the $t1$ level in $t4$. A lower roll neuromuscular frequency indicates that pilots act on less high-frequency disturbances during the approach to stall and the dive portion of the stall task. The pilot time delay was smaller in the EH and FM conditions compared to the NM and GH conditions by around 60 ms. A possible explanation for this is that the increased motion made it easier for pilots to act quicker on the disturbances.

In the pitch axis, the pilot position gain K_p showed a different behavior compared to roll. Motion did not introduce any significant change; however, at $t3$ the pilot position gain significantly decreased, probably due to the large pitch attitude change at the end of the dive maneuver, which made pilots control more carefully in pitch in this time segment compared to the other time segments. The pitch velocity gain was the highest for the FM condition, unlike the roll axis where the highest K_v was obtained for the EH condition. Unlike the roll neuromuscular frequency, the pitch neuromuscular frequency was significantly affected by the motion condition, which is an interesting find. The lowest pitch ω_n was obtained for the EH condition, the next highest neuromuscular frequency was obtained for the NM condition, then the GH condition, and the highest pitch ω_n was found for the FM condition. This order cannot be readily explained. Similar to the roll axis, the neuromuscular frequency in the pitch axis seems to decrease in the $S2$ and $S3$ segments compared to the $S1$ and $S4$ segments. The neuromuscular damping ratio in the pitch axis is the highest overall for the GH condition, followed by the FM condition and then the NM and EH motion conditions. These differences are the largest in $S1$. At the end of the stall recovery task, neuromuscular damping is more similar for all motion conditions. The pilot time delay in the pitch axis is the lowest for the EH condition. The highest time delay is found for the NM task, an expected result. However, unlike the roll axis, the pilot time delay is similar under the GH and FM motion configurations.

The roll crossover frequency was higher for the conditions with motion compared to the no motion condition. It was the lowest at the end of $S3$, most likely due to the slightly decreased stability of the aircraft as indicated by the lower aircraft dynamics break frequency in Fig. 13b. The roll phase margin was highest for the EH condition and at $t2$, as was expected since the aircraft roll dynamics were the most stable at $t2$. In the pitch axis, the crossover frequency was the highest for the full-motion condition FM. The pitch crossover frequency was the lowest at the end of $S3$, probably due to the large pitch attitude change, resulting in pilots not compensating for disturbances effectively, despite the fact that the pitch dynamics were the most unstable at the end of $S2$ (Fig. 14b). It is also interesting to note that the largest difference between motion conditions occurred at $t3$. Possibly indicating that the motion condition affects pitch open-loop performance the most where the aircraft response is more dynamic. Pitch phase margin was the lowest for the EH condition and not the FM condition. It was the highest at $t3$, although the aircraft dynamics were more stable at $t4$ (Fig. 14b). A possible explanation could be that the low pitch dynamics gain at $t3$ resulted in an increase in open-loop phase margin.

The DEKF did provide accurate estimation results in both the roll and pitch axes. However, more accurate and consistent results were obtained in roll compared to pitch, confirming hypothesis H1. Especially the pilot pitch neuromuscular parameters showed behavior unlikely caused solely by the motion condition that cannot be readily explained.

Hypothesis H2 can be partially accepted, as the effects of motion on pilot control behavior and performance in roll were in line with previous research, but less so in pitch. The pilot position gain K_v was the lowest in the NM condition for both axes, and the highest in EH for the roll axis and FM for the pitch axis. Furthermore, the pilot position gain did not significantly change for the roll axis but did for the pitch axis. The differences in pilot velocity gain were much smaller between the NM, GH and EH conditions for the pitch axis compared to the roll axis. Finally, disturbance-rejection performance was more significantly affected by motion in roll compared to pitch. These findings provide useful insights into how different simulator motion settings affect pilot control behavior differently depending on the controlled axis. However, this obviously also depends on the type of task.

Pilot control behavior and performance significantly adapted as the aircraft dynamics changed throughout the stall task. Mainly the pilot equalization parameters changed over time. The pilot velocity gains increased closer to the stall point. Pilot position gains remained fairly constant between $t1$ and $t2$ but decreased in the stall recovery. This means H3 can be accepted. Finally, hypothesis H4 can be accepted as differences between motion configurations in most dependent variables increased closer to the stall point. A very clear example of this effect can be observed in the pilot roll position and velocity gains (comparing $t1$ and $t2$), and the disturbance-rejection performance in roll and pitch.

VI. Conclusion

A stall recovery task experiment was performed in the Vertical Motion Simulator at NASA Ames Research Center. Pilots had to follow a flight director into a stall and then into a recovery maneuver. Disturbances were added in both the pitch and roll axes in order to identify manual control parameters during different stages of the task using a novel time-varying parameter estimation method. Four simulator motion conditions were used: no motion, generic hexapod motion, enhanced hexapod motion, and full motion. Performance was highest for the enhanced hexapod and full motion conditions in both axes and the lowest for the condition with no motion. In the roll axis, the pilot position gain did not significantly change between time segments, but was the lowest for the condition with no motion. The pilot velocity gain was significantly different between motion conditions, the largest difference being found just before the stall point. The enhanced hexapod motion condition induced the highest pilot roll velocity gain. In the pitch axis, the pilot position gain was significantly different between time segments but not between motion conditions. The pilot pitch velocity gain was highest for the full motion condition and increased at the beginning of the stall, but did not change significantly for the other motion conditions. Neuromuscular frequency decreased for both roll and pitch axes at the beginning of the stall and in the recovery. There was no difference between motion conditions in the roll axis, unlike the pitch axis where significant differences in neuromuscular frequency were found. In summary, these findings suggest that the enhanced hexapod motion configuration induced pilot control behavior and performance more similar to that under the full motion configuration, but more so in roll compared to pitch. Furthermore, the different motion configurations affected control behavior and performance more strongly at different times during the stall maneuver; for example, close to the stall point. This might warrant the use of adaptive motion algorithms that emphasize different components of the total aircraft motion throughout a stall.

Acknowledgements

The authors thank everyone at NASA Ames SimLabs who contributed to the experiment. We especially thank Steven Norris and Emily Lewis for their daily support in setting up the experiment and operating the Vertical Motion Simulator. We thank the pilots who participated in the experiment. Finally, we would also like to thank Dr. Thomas Lombaerts for his help and support during the initial setup of the experiment. This work was supported by NASA's Technologies for Airplane State Awareness project for which Dr. Gautam Shah is the technical program coordinator.

References

[1]Federal Aviation Administration, *Stall Prevention and Recovery Training*, Nov. 2015, Advisory Circular 120-109A.

[2]Schroeder, J. A., "Research and Technology in Support of Upset Prevention and Recovery Training," *Proceedings of the AIAA Modeling and Simulation Technologies Conference, Minneapolis (MN)*, No. AIAA-2012-4567, 13–16 Aug. 2012.

[3]McRuer, D. T. and Jex, H. R., "A review of quasi-linear pilot models," *Human Factors in Electronics, IEEE Transactions on*, , No. 3, 1967, pp. 231–249.

[4]Stapleford, R. L., Peters, R. A., and Alex, F. R., "Experiments and a Model for Pilot Dynamics with Visual and Motion Inputs," Tech. Rep. NASA CR-1325, NASA, 1969.

[5]Zaal, P. M. T., Pool, D. M., de Bruin, J., Mulder, M., and van Paassen, M. M., "Use of Pitch and Heave Motion Cues in a Pitch Control Task," *Journal of Guidance, Control, and Dynamics*, Vol. 32, No. 2, March–April 2009, pp. 366–377.

[6]Pool, D. M., Zaal, P. M. T., van Paassen, M. M., and Mulder, M., "Effects of Heave Washout Settings in Aircraft Pitch Disturbance Rejection," *Journal of Guidance, Control, and Dynamics*, Vol. 33, No. 1, Jan.–Feb. 2010, pp. 29–41.

[7]Schroeder, J. A. and Grant, P. R., "Pilot Behavioral Observations in Motion Flight Simulation," *Proceedings of the AIAA Guidance, Navigation, and Control Conference and Exhibit, Toronto (ON), Canada*, No. AIAA-2010-8353, 2–5 Aug. 2010.

[8]Zaal, P., Popovici, A., and Zavala, M. A., "Effects of False Tilt Cues on the Training of Manual Roll Control Skills," *AIAA Modeling and Simulation Technologies Conference*, 2015, p. 0655.

[9]Klyde, D. H., Thompson, P. M., Bachelder, E. N., and Rosenthal, T. J., "Evaluation of Wavelet-Based Techniques for Detecting Loss of Control," *Proceedings of the AIAA Atmospheric Flight Mechanics Conference and Exhibit, Providence (RI)*, No. AIAA-2004-4702, 16–19 Aug. 2004.

[10]Olivari, M., Nieuwenhuizen, F. M., Bülthoff, H. H., and Pollini, L., "Identifying Time-Varying Neuromuscular Response: Experimental Evaluation of a RLS-based Algorithm," *Proceedings of the AIAA Modeling and Simulation Technologies Conference, Kissimmee, Florida FL*, No. AIAA-2015-0658, 5–9 Jan. 2015.

[11]Zaal, P. M., "Manual Control Adaptation to Changing Vehicle Dynamics in Roll–Pitch Control Tasks," *Journal of Guidance, Control, and Dynamics*, 2016, pp. 1046–1058.

[12]van Grootheest, A., Pool, D. M., van Paassen, M., and Mulder, M., "Identification of Time-Varying Manual Control Adaptations with Recursive ARX Models," *2018 AIAA Modeling and Simulation Technologies Conference*, No. AIAA-2018-0118, American Institute of Aeronautics and Astronautics, jan 2018.

[13]Popovici, A., Zaal, P. M. T., and Pool, D. M., "Dual Extended Kalman Filter for the Identification of Time-Varying Human Manual Control

Behavior," *AIAA Modeling and Simulation Technologies Conference*, No. AIAA-2017-3666, American Institute of Aeronautics and Astronautics, jun 2017.

[14]Hueschen, R. M., "Development of the Transport Class Model (TCM) Aircraft Simulation From a Sub-Scale Generic Transport Model (GTM) Simulation," Technical Report NASA/TM–2011-217169, NASA Langley Research Center, Hampton, Virginia, 2011.

[15]Hyde, D. C., Brown, F. R., Shweyk, K. M., and Shah, G. H., "Advanced Modeling and Uncertainty Quantification for Flight Dynamics (VSST1-7) Interim Results and Challenges," *AIAA Atmospheric Flight Mechanics Conference*, No. AIAA-2014-0035, American Institute of Aeronautics and Astronautics, jan 2014.

[16]Lombaerts, T., Schuet, S., Stepanyan, V., Kaneshige, J., Hardy, G., Shish, K. H., and Robinson, P., "Piloted Simulator Evaluation Results of Flight Physics Based Stall Recovery Guidance," *2018 AIAA Guidance, Navigation, and Control Conference*, No. AIAA-2018-0383, American Institute of Aeronautics and Astronautics, jan 2018.

[17]Campbell, S., Kaneshige, J., Nguyen, N., and Krishnakumar, K., "An Adaptive Control Simulation Study using Pilot Handling Qualities Evaluations," *AIAA Guidance, Navigation, and Control Conference*, No. AIAA-2010-8013, American Institute of Aeronautics and Astronautics, aug 2010.

[18]Steurs, M., Mulder, M., and van Paassen, M. M., "A Cybernetic Approach to Assess Flight Simulator Fidelity," *Proceedings of the AIAA Modelling and Simulation Technologies Conference and Exhibit, Providence (RI)*, No. AIAA-2004-5442, 16–19 Aug. 2004.

[19]McRuer, D. T., Graham, D., Krendel, E. S., and Reisener, W., "Human Pilot Dynamics in Compensatory Systems. Theory, Models and Experiments With Controlled Element and Forcing Function Variations," Tech. Rep. AFFDL-TR-65-15, Wright Patterson AFB (OH): Air Force Flight Dynamics Laboratory, 1965.

[20]Zaal, P. M. T. and Mobertz, X. R. I., "Effects of Motion Cues on the Training of Multi-Axis Manual Control Skills," *AIAA Modeling and Simulation Technologies Conference*, AIAA, Denver, Colorado, 2017.

[21]Beard, S. D., Reardon, S. E., Tobias, E. L., and Aponso, B. L., "Simulation System Optimization for Rotorcraft Research on the Vertical Motion Simulator," *Proceedings of the AIAA Modeling and Simulation Technologies Conference, Minneapolis (MN)*, No. AIAA-2012-4634, 13–16 Aug. 2012.

[22]International Civil Aviation Organization, *ICAO 9625: Manual of Criteria for the Qualification of Flight Simulation Training Devices. Volume 1 – Aeroplanes*, 2009, 3rd edition.

[23]Zaal, P. M. T., Pool, D. M., Chu, Q., Mulder, M., Van Paassen, M., and Mulder, J. A., "Modeling Human Multimodal Perception and Control using Genetic Maximum Likelihood Estimation," *Journal of Guidance, Control, and Dynamics*, Vol. 32, No. 4, 2009, pp. 1089–1099.

[24]Shirley, R. S. and Young, L. R., "Motion Cues in Man-Vehicle Control," *Fourth Annual NASA-University Conference on Manual Control*, University of Michigan, Ann Arbor (MI), 21–23 March 1968, pp. 435–448.